

Neutron and Gamma-Ray Spectra from a Variety of Materials Bombarded with 14-MeV Neutrons

E. Goldberg, L. F. Hansen, T. T. Komoto, B. A. Pohl, R. J. Howerton, R. E. Dye, E. F. Plechaty & W. E. Warren

To cite this article: E. Goldberg, L. F. Hansen, T. T. Komoto, B. A. Pohl, R. J. Howerton, R. E. Dye, E. F. Plechaty & W. E. Warren (1990) Neutron and Gamma-Ray Spectra from a Variety of Materials Bombarded with 14-MeV Neutrons, Nuclear Science and Engineering, 105:4, 319-340, DOI: [10.13182/NSE90-A21468](https://doi.org/10.13182/NSE90-A21468)

To link to this article: <https://doi.org/10.13182/NSE90-A21468>



Published online: 13 May 2017.



Submit your article to this journal



Article views: 9



Citing articles: 5 [View citing articles](#)

Neutron and Gamma-Ray Spectra from a Variety of Materials Bombarded with 14-MeV Neutrons

E. Goldberg, L. F. Hansen, T. T. Komoto, B. A. Pohl, R. J. Howerton,
R. E. Dye, E. F. Plechaty, and W. E. Warren

Lawrence Livermore National Laboratory, P.O. Box 808
Livermore, California 94551

Received April 26, 1989

Accepted August 25, 1989

Abstract—Measurements of the neutron and gamma-ray leakage spectra from 15 spherical target assemblies (carbon, nitrogen, H_2O , C_2F_4 , aluminum, silicon, titanium, iron, copper, tantalum, tungsten, gold, lead, ^{232}Th , and ^{238}U) pulsed with 14-MeV neutrons were made using time-of-flight techniques. The spheres were $\sim 30\text{ g/cm}^2$ thick to maximize the gamma-ray leakage per central source neutron. Among all the materials studied, silicon shows the highest conversion factor ($\sim 2\text{ \gamma MeV/n}$), and lead the lowest (0.31 \gamma MeV/n). Monte Carlo neutron-photon transport calculations were done using the TART and SANDYL codes, with the ENDL and ENDF/B-V libraries. Comparisons with the neutron measurements confirm earlier results, where both libraries reproduced the leakage spectra for most of these materials reasonably well. The gamma spectra calculated with ENDL give a fair representation of the measurements, with the exception of the initial calculations for $^{16}O(H_2O)$ and $^{19}F(C_2F_4)$, where serious discrepancies are found. Improvements were obtained for ^{16}O after a re-evaluation of the neutron-induced cross sections based on more recent microscopic experimental data. This was also the case for ^{19}F , where the calculations now overestimate the measurements by 30%. Calculations with the ENDF/B-V are lower than the experimental measurements for most of the materials.

INTRODUCTION

Nuclear power systems can benefit from the use of large, computer-based models to optimize their overall design. These models depend on the completeness of the physical and mathematical assumptions and the quality of the nuclear data base used. A wide variety of tests to ensure the validity of the code results are desirable.

This paper illustrates benchmark experiments in which neutrons and gamma rays generated by 14-MeV neutrons in a host of materials yielded data that reflect the nature of the effluent. We performed Monte Carlo calculations using two independent sets of evaluated nuclear cross sections, and we searched the literature for additional microscopic cross-section data. Through this procedure, we hoped to arrive at a more realistic view of the predictive capabilities of our computational model. In our calculations, we used the TART code,¹ with which we generated the secondary neutron and

gamma-ray leakage spectra. We then used the output gamma rays as input spectra in the SANDYL Monte Carlo calculations,² which are necessary to predict the detector response. For the TART calculations, we used two independent evaluations: Lawrence Livermore National Laboratory's (LLNL's) ENDL (Ref. 3) and ENDF/B-V (Ref. 4).

By comparing the measured neutron and gamma-ray leakage spectra to calculations, we obtained a stringent test of the predictions. As an example, we considered inelastic neutron scattering. After scattering, the residual nucleus may deexcite via gamma-ray cascade. On the other hand, if the excited nucleus is charged-particle unstable, much of the excess energy may be consumed in the transmutation, and a smaller amount of energy would appear as gamma rays. The dual measurements clearly help to clarify the deexcitation process.

The materials studied were carbon, nitrogen, H_2O , C_2F_4 , aluminum, silicon, titanium, iron, copper,

tantalum, tungsten, gold, lead, ^{232}Th , and ^{238}U . We chose the assemblies through which neutrons generated at the center of the spherical assembly would go to be between 30 and 40 g/cm² in density. Previous Monte Carlo calculations demonstrated that such a size would maximize the gamma-ray leakage signal. We determined the choice of targets generally to provide a representative host of common materials found in the design of fusion and hybrid reactors and air transport problems.

The main objective of this work was to measure the gamma-ray leakage spectra because we have already done extensive measurements of the neutron spectra. (See Ref. 5 for a list of measurements and publications under the pulsed-sphere program.) However, we repeated the neutron measurements for the present assemblies because we decided that, by simultaneously measuring the gamma and neutron spectra (a common 14-MeV neutron source and detector, under the same experimental conditions), the neutron spectra would help us to understand any discrepancies found in comparing the measured and calculated gamma spectra. In the past, we had done gamma measurements^{6,7} for nitrogen, ^{232}Th , and ^{238}U . We repeated them here because of the availability of better time resolution and energy calibration. Furthermore, the use of the SANDYL code in the transformation of the gamma spectra calculated by TART to the electron recoil spectra (ERS) obtained with the NE-213 detector was an improvement over the simplified calculational model used earlier.

EXPERIMENTAL PROCEDURE

The simple geometry of the experimental setup⁸ allows for a detailed description in the computational model. The 14-MeV neutron source was housed in a low-mass structure, and each assembly was slipped over the source so that neutrons were produced in the central region of the assembly. The 14-MeV neutrons were generated by the $\text{T}(d, n)^4\text{He}$ reaction, using the 400-keV D^+ beam from the recently decommissioned insulated-core transformer accelerator at LLNL.

The beam was swept and bunched with a repetition rate of 0.5 MHz and a burst width of $\sim 2/\text{ns}$. A solid-state detector, permanently positioned on the low-mass structure at 174 deg with respect to the D^+ beam line, monitored neutron production by counting the associated ^4He particles. We used a proton recoil counter of known absolute calibration⁹ for all runs to provide an accurate measurement of the neutron fluence and to compare it with the one from the alpha-particle detector. The details of the low-mass structure are given in Ref. 8. The tritium was absorbed on a 1.59-cm diam, nominally 4 mg/cm² thick titanium layer evaporated on a 0.076-cm-thick tungsten disk. The beam spot size was ~ 1.0 cm in diameter.

Most of the targets were solid spheres (Fig. 1a) accurately described by four parameters: R_1 (radius of the sphere), D (diameter of the bottom of the source well), δ (distance between the center of the sphere and bottom source well), and α (angle between the deuteron beam line and sides of the source well). In the silicon assembly, we replaced the flat bottom of the source well with a hemispherical shape (Fig. 1b), anticipating a smaller uncertainty in the geometric modeling of the spherical assembly. The tungsten assembly was a nest of spherical shells, with a total thickness of 2.54 cm. Table I provides a detailed description of all the assemblies, except for the H_2O flask and the liquid nitrogen dewar, which are depicted in Figs. 1c and 1d, respectively.

Neutrons and gamma rays were detected by a nominal 5.1-cm-diam \times 5.1-cm-long NE-213 scintillator detector, using time-of-flight (TOF) and pulse-shape discrimination to distinguish between neutrons and gamma rays. Figure 2 illustrates the gamma-neutron separation typically obtained in these measurements. The center of the detector was 852.5 cm from the neutron source for all experiments. The detector bias was set at one-half of the 0.51-MeV ^{22}Na line, which corresponds to a 0.17-MeV electron energy. Each spherical target assembly, centered in a large room, was visible to the detector positioned in another room through a 20.2-cm-diam iron collimator surrounded by a water liner that filled the annular space in a 197-cm-thick concrete wall.

Data were taken in two series spaced 1 yr apart. Using two similar detectors, we x-rayed each scintillator assembly to accurately determine the dimensions of the housing and the size of the inert gas bubble in its scintillator fluid chamber. Both contained 96.0 cm³ of fluid with a density of 0.874 g/cm³. One bubble was 6.7 cm³, and the other was 5.8 cm³. These details were carefully described in the corresponding SANDYL calculations. The chemical composition of the NE-213 was taken to be $\text{C}_{45}\text{H}_{55}$.

For neutrons, we used our customary calibration procedure.⁸ The resultant analysis led to a neutron TOF spectrum that was effectively normalized to the "blank," or sphereless, neutron spectrum. For gamma rays, on the other hand, we obtained an absolute calibration using calibrated gamma sources.

GAMMA-RAY DETECTOR CALIBRATION

The NE-213 detector calibration for gamma rays followed our earlier procedure.^{6,7} We exposed the detector under controlled conditions to various calibrated gamma-ray sources and generated pulse-height distributions resulting from Compton, photoelectric, and pair production events in the materials of the detector. The response of the NE-213 detector to the gamma-ray fluence was calculated with the SANDYL code.²

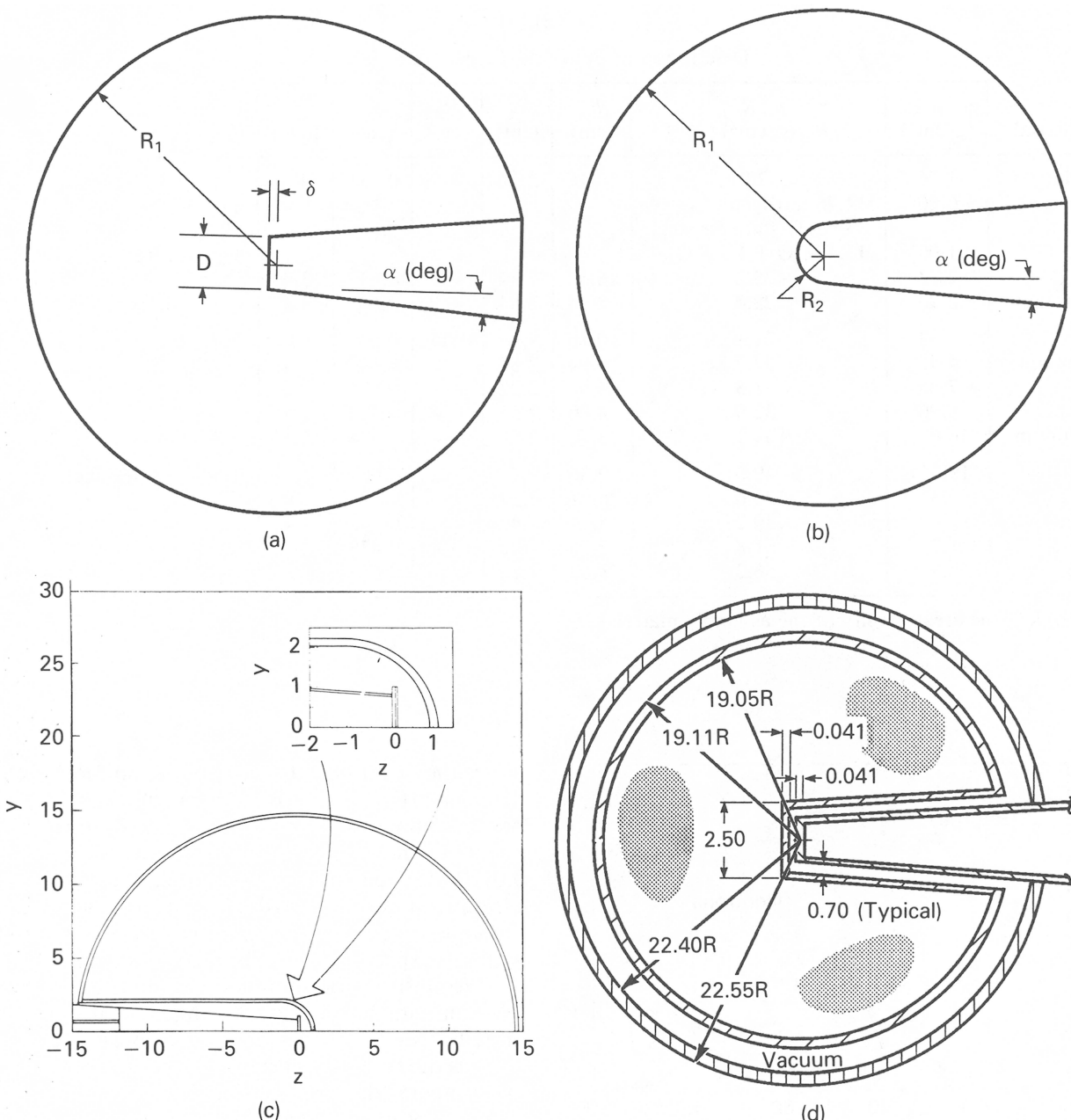


Fig. 1. Spherical targets: (a) typical geometry, (b) silicon assembly (the tungsten shell is also described by the same set of parameters), (c) H_2O flask, (d) dewar vessel filled with liquid nitrogen. All dimensions are in centimetres.

The calibrated sources were ^{22}Na , ^{24}Na , ^{137}Cs , and ^{60}Co ; in addition, we used $\text{Pu}-^9\text{Be}(\text{C})$, ^{228}Th , and $\text{Pu}-^{13}\text{C}(\text{O})$ sources to study the linearity of the detector to higher energy gamma rays. A careful examination of the observed Compton cutoff and double escape peak showed that the Compton cutoff energy coincided with that point of the ERS where the count rate fell to 80% of the Compton peak. Using this criterion and modifying¹¹ the phototube base, we found the detector response to be linear for $0.34 \leq E_\gamma \leq 6.13$ MeV.

We performed ERS calculations¹⁰ for each of the above sources with the SANDYL code. We carefully modeled the detector and specified that its 22.8-cm² face, which included the aluminum sidewall, was illuminated by the gamma rays from the disk-shaped sources.

For calculations coupling TART and SANDYL, we assumed the detector to be uniformly illuminated, which introduced an error of <1% in source strength. The code generated an energy distribution over 100 equal energy increments. With the energy calibration

TABLE I
Description of Spherical Target Assemblies

Material	ρ (g/cm ³)	$\rho\Delta R^a$ (g/cm ²)	R_1 (cm)	D (cm)	R_2 (cm)	δ (cm)	α (deg)	Comments
Carbon	1.76	17.71	10.16	2.26	---	0.131	4.0	
Nitrogen	0.808	14.76 nitrogen + 2.31 stainless steel						Fig. 1d, Ref. 8 for details
H ₂ O	1.00	13.4 H ₂ O + 1.1 SiO ₂						Fig. 1c, Ref. 10 for details
C ₂ F ₄	2.22	35.2	16.50	2.84	---	0.64	3.4	
Aluminum	2.70	22.4	8.94	2.84	---	0.64	3.4	
Silicon	2.33	21.1	10.16	---	1.11	0.00	4.0	Fig. 1b
Titanium	4.45	37.7	8.94	2.84	---	0.64	3.4	
Iron	7.85	31.3	4.46	2.22	---	0.475	4.0	
Copper	8.96	32.9	4.00	2.55	---	0.324	1.5	
Tantalum	16.6	51.1	3.40	2.54	---	0.324	1.5	
Tungsten	19.3	49.0	10.36	---	7.82	0.00	---	
Gold	19.3	120.0	6.21	2.54	---	0.00	4.0	
Lead	11.3	59.2	5.56	2.40	---	0.340	3.4	
²³² Th	11.7	61.8	5.76	2.22	---	0.475	4.0	
²³⁸ U	17.8	56.2	3.63	2.22	---	0.475	4.0	

^a $\rho\Delta R$ is the areal density of the assembly material.

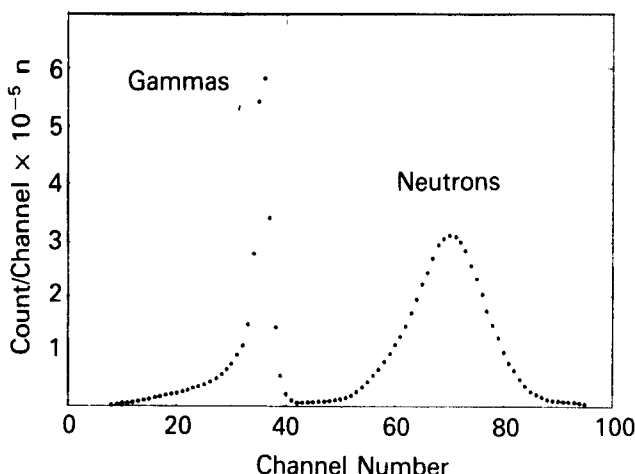


Fig. 2. Typical gamma-neutron separation obtained with pulse-shape discrimination circuitry.

obtained from the sources, the SANDYL distribution was converted to the measured ERS in counts per channel:

$$\frac{\text{counts}}{\text{electron MeV} \cdot \text{photon}} \times (22.8 \text{ cm}^2) \times \frac{\text{photons}}{\text{cm}^2} \times \frac{\text{conversion factor}}{1.10} = \frac{\text{counts}}{\text{channel}}, \quad (1)$$

where the quantity 1.10 is the correction factor for the detector efficiency derived from the runs with calibrated gamma-ray sources and, for most of the experiments in the second series, the conversion factor is 0.0120 MeV/channel. We smoothed the calculations, assuming a normal distribution function and varying the standard deviation until the calculated ERS agreed with the experimentally observed shape.

We illustrate the gamma-ray calibration procedure by examining an exercise in which an absolute calibrated ²⁴Na source was accurately positioned along the axis of the NE-213 detector. Figure 3 compares the experimental data to the SANDYL-generated ERS. The Compton edges from the two lines, at 1.369 and 2.754 MeV, are observed together with the double escape peak. The SANDYL code gives a good overall representation of the measured spectra. For ²⁴Na, a standard deviation of 0.025 in the smoothing operation gave a good fit between experiment and SANDYL calculation, and the conversion factor was 0.00841 MeV/channel.

For the first series of pulsed-sphere experiments, the net correction factor for the ratio of calculated-to-experimental (C/E) ERS, based on all the calibration runs, was 1.05 ± 0.04 . The corresponding number for the second series was 1.10 ± 0.04 , based on an independent set of calibrations performed some days before the start of the second series. The uncertainty represents the variation in the ratio of C/E counts per channel inferred from the various sources.

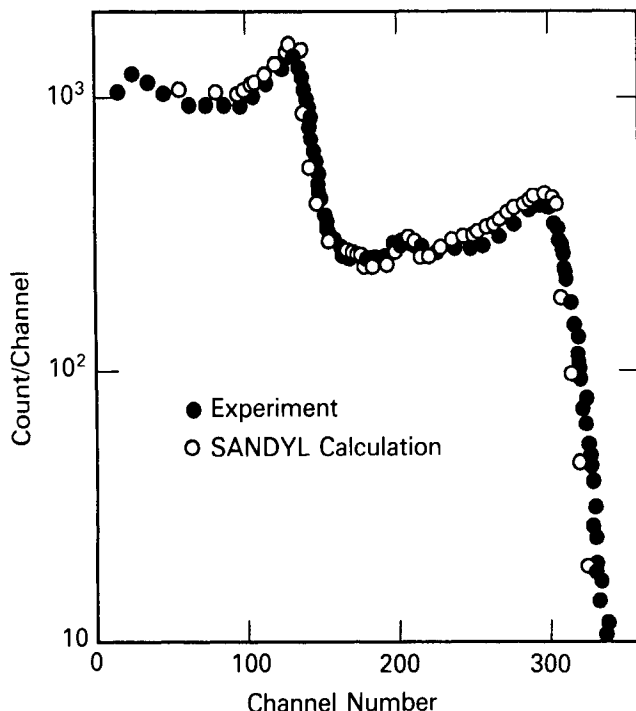


Fig. 3. Comparison of SANDYL-generated ERS to its experimental counterpart resulting from exposure of NE-213 scintillator detector to a calibrated ^{24}Na gamma-ray source.

CALCULATIONS

This study was primarily an exercise to assess the degree and range of validity of the TART code and its associated data files by comparing the code output to experimental data. For leakage neutrons, a simple edit of the TART output, incorporating the detector efficiency and time resolution of the measurements, permitted a straightforward comparison.⁸ For gamma-ray leakage, however, we examined the spectrum by explicitly studying the resultant calculated ERS. After passing the gamma spectrum generated by TART through a test surface at the detector position, we edited it to generate an input spectrum for the SANDYL code. The main function of this edit code (NEWEPS) is to reject gamma rays entering the test surface at too oblique an angle because the iron collimator restricts the detector's field of view. The edit also rejected gamma rays falling outside the detector acceptance time. Typically, 15 to 20% of the gamma rays interrogated were rejected as a result of these two tests.

The TART input descriptions guaranteed inclusion of the air attenuation of neutrons and gamma rays. The collimator was not explicitly incorporated, but the effluent neutrons and gamma rays that failed the collimator criterion ($\theta \leq R_T/852.5$) were rejected (R_T is the radius of the field of view seen by the detector at an axial distance of 852.5 cm). For smaller targets, $R_T = 15$ cm to allow inclusion of particles that might

scatter by interaction with the air in the immediate vicinity of the spherical assemblies.

Among the possible sources of background were electrons generated by gamma rays interacting with the air in the target room and collimator. We performed several SANDYL calculations to assess this effect, which was found to be $\leq 1\%$ of the main signal.

We now briefly outline the procedure to calculate the ERS recorded by the NE-213 detector from the TART/SANDYL results. First, we determined the neutron source strength for each experiment. We intermixed frequent blank runs (no spherical assembly) among the measurements of the targets to ensure reproducibility of the electronic system and provide a reliable measure of the neutron fluence through the proton recoil counter response. We had previously calibrated the proton recoil counter with respect to the $^{27}\text{Al}(n, \alpha)^{24}\text{Na}$ reaction.⁹ The alpha counter that viewed the deuterium-tritium (D-T) source served as a calibrated source for the experiments with target assemblies in place because the proton recoil counter response was affected by the presence of the assemblies. The responses of the proton recoil and alpha counters during the blank runs agreed very well. We also corrected the neutron fluence for a 6% anisotropy.¹²

We then edited the TART calculation, which closely modeled the experiment under examination, for $\sim 8 \times 10^5$ particle histories. The collimator effect was simulated by applying the two rejection criteria to the gamma rays that crossed a portion of a spherical surface at the detector position. This edit procedure, together with the neutron source strength (obtained from the blank runs), allowed us to determine the gamma-ray fluence with its energy spectrum in 64 equally probable bins at the detector station.

Once the gamma-ray fluence impinging on the face of the NE-213 detector was obtained, we calculated the ERS with SANDYL. This calculation proceeded in the same manner as the ERS calculated for the gamma sources.

PREPARATION AND CONVERSION OF ENDF/B-V DATA BASE INTO TART FORMAT

We converted the evaluated data files to the form and format required for the TART code by the sequential use of two processing codes. The first code uses a library in the ENDL binary format as part of its input. The second uses the output of the first and an existing TART data file that is updated with the new processed data.

To deal with the ENDF/B-V library, we had two choices. Either we could build new processing codes that could use the ENDF/B-V data directly to produce TART data files, or we could translate the ENDF/B-V data into the ENDL input format and make a new library that the existing processing codes could operate

on. We chose the latter. Neither of the procedures would have been trivial, but our choice seemed to be the least subject to error. While processing codes were available from other laboratories, none produced processed data in the format required by TART.

The two systems differ both in units and forms permitted for representing the microscopic data. In the early days of the ENDF/B-V files, after we received the data in a trial format called ENDF/C, we wrote a code that translated the data to the ENDL format. The ENDF/C format was used in all our earlier publications where calculations with ENDF/B-V were reported.

For this work, we decided that calculations using the version V data should be done with the ENDF/B-V data directly rather than trying to use the ENDF/C format, where errors were uncovered in the course of time. Consequently, new data files were obtained from the National Nuclear Data Center at Brookhaven National Laboratory, and a code was written to translate data directly from ENDF/B-V to ENDL format. The translated data were carefully checked against the ENDF/B form whenever a direct check was possible and, for several materials, were retranslated to the ENDF/B format and compared whenever a comparison could be made. The translated data were then processed to make TART data files of the ENDF/B-V evaluated data. The versions of the ENDF/B-V data were those current in the September 1987 files (e.g., the iron data were those of Revision 2 of MAT 1326).

EXPERIMENTAL RESULTS AND CALCULATIONS

The neutron TOF and ERS spectra are given for each material studied in this work. The calculated curves were obtained with the TART/SANDYL codes, once using the latest (April 28, 1988) ENDL cross-section set and a second time using the ENDF/B-V set. The comparisons between measurements and calculations shown in Figs. 5 through 19 not only show the quality of the agreement found in these comparisons but also reveal the discrepancies between the two sets of cross sections. In addition to the 15 materials investigated, we also compared the results of these experiments with the calculations of the spectra extracted from a typical blank run (Fig. 4).

In all the measurements, the detector was biased at one-half of the energy of the 0.511-MeV gamma-ray line from ^{22}Na , or 0.25 MeV. In the TOF figures, a scale parallel to the abscissa shows the neutron energy corresponding to the TOF. Similarly, in the ERS figures, the scale corresponding to the Compton cutoff energies is also shown. The relationship between the cutoff energy E_e and photon energy E_γ is

$$E_e = E_\gamma (1 + 0.2555/E_\gamma)^{-1} . \quad (2)$$

We chose, as a measure of gamma-ray energy deposition in the NE-213 detector, the quantity $\Sigma n_i C_i$, where C_i is the channel number and n_i is the number of electron counts per source neutron count in channel i . In fact, C_i is not exactly proportional to the electron energy deposited. For example, when we studied the detector linearity in the second series of experiments, we found that the relationship between electron energy deposition E_i and channel number was

$$C_i = \frac{(E_i - c_1)}{c_2} = \frac{E_i - 0.033}{0.0120} . \quad (3)$$

This relation between channel number and energy would imply an $\sim 4\%$ adjustment of the sum $\Sigma n_i C_i$ for the materials studied.

We took care to account for the bias setting of the detector in determining $\Sigma n_i C_i$ so that the comparisons of the summations among different materials had a common basis. The lower limit of the electron energy in these summations was 0.17 MeV, the value that corresponds to the gamma-ray energy bias setting of 0.255 MeV used in all the measurements. Table II summarizes the neutron TOF findings for the 15 materials studied, along with a typical blank run. The values of $\Sigma n_i C_i$ obtained from the gamma-ray measurements and from calculations with the ENDL and ENDF/B-V libraries are listed in Table III for each material. For those materials whose measurements were repeated between the first and second series of experiments, the average value of $\Sigma n_i C_i$ has been tabulated.

Blank

The measured neutron TOF spectrum and those calculated with the ENDL and ENDF/B-V libraries are compared in Fig. 4a for a typical blank run. The agreement between the experiment and both calculations is fairly good. The small peak at 350 ns is a result of deuterium buildup in the tritiated target and amounts to $\ll 1\%$ of the D-T neutrons. The dip in the ENDF/B-V curve at ~ 2 MeV is probably a result of poor statistics. The integrals (count/source neutron count) for the neutron emission spectra corresponding to three energy intervals (15 to 10, 10 to 5, and 5 to 1.2 MeV; hereafter called high-, medium-, and low-energy intervals) are listed in Table II, together with the C/E ratios.

Figure 4b compares the measured ERS and the calculations. Agreement between the experiment and the ENDL-based calculations is quite good. In Table III, C/E = 1.00 with ENDL cross sections, and C/E = 0.90 with an ENDF/B-V base.

To assess the nature of the background, we performed a separate experiment in which a copper shadow bar was interposed between the neutron source and the detector. The shadow-shielded gamma-ray signal was found to be 7% of the blank signal for gamma rays. The photon source edit in TART using an ENDL data base shows a total of 0.27 γ MeV/n, with the

TABLE II

Measured and Calculated Neutron Integrals* and Ratios of Calculated-to-Measured Integrals

Material	Energy (MeV)	E ^a	C ₁ ^b	C ₂ ^c	(C ₁ /E)	(C ₂ /E)	C ₁ /C ₂
Blank	15.0 to 10.0	1.002	1.019	1.019	1.02	1.02	1.00
	10.0 to 5.0	0.008	0.008	0.009	1.00	1.12	0.89
	5.0 to 1.2	0.037	0.026	0.032	0.70	0.86	0.81
Carbon	15.0 to 10.0	0.598	0.590	0.604	0.99	1.01	0.98
	10.0 to 5.0	0.154	0.128	0.148	0.83	0.96	0.86
	5.0 to 1.2	0.195	0.185	0.148	0.95	0.76	1.25
Nitrogen	15.0 to 10.0	0.682	0.617	0.640	0.91	0.94	0.97
	10.0 to 5.0	0.077	0.086	0.083	1.12	1.08	1.04
	5.0 to 1.2	0.160	0.181	0.176	1.12	1.11	0.99
H ₂ O	15.0 to 10.0	0.440	0.461	0.447	1.05	1.02	1.03
	10.0 to 5.0	0.128	0.131	0.127	1.02	0.99	1.03
	5.0 to 1.2	0.162	0.173	0.151	1.07	0.93	1.15
C ₂ F ₄	15.0 to 10.0	0.380	0.364	0.382	0.96	1.00	0.96
	10.0 to 5.0	0.112	0.097	0.112	0.86	1.00	0.86
	5.0 to 1.2	0.287	0.297	0.313	1.03	1.09	0.94
Aluminum	15.0 to 10.0	0.620	0.591	0.572	0.95	0.92	1.03
	10.0 to 5.0	0.066	0.068	0.070	1.03	1.07	0.97
	5.0 to 1.2	0.235	0.230	0.252	0.98	1.07	0.91
Silicon	15.0 to 10.0	0.675	0.640	0.662	0.95	0.98	0.92
	10.0 to 5.0	0.055	0.035	0.046	0.64	0.83	0.77
	5.0 to 1.2	0.190	0.190	0.132	1.00	0.69	1.45
Titanium	15.0 to 10.0	0.556	0.589	0.541	1.06	0.97	1.09
	10.0 to 5.0	0.056	0.045	0.069	0.81	1.22	0.66
	5.0 to 1.2	0.353	0.295	0.307	0.84	0.87	0.96
Iron	15.0 to 10.0	0.632	0.653	0.626	1.03	0.99	1.04
	10.0 to 5.0	0.047	0.045	0.053	0.97	1.13	0.86
	5.0 to 1.2	0.270	0.239	0.252	0.88	0.93	0.95
Copper	15.0 to 10.0	0.635	0.626	0.629	0.99	0.99	1.00
	10.0 to 5.0	0.042	0.025	0.043	0.58	1.01	0.58
	5.0 to 1.2	0.278	0.221	0.276	0.80	1.00	0.80
Tantalum	15.0 to 10.0	0.711	0.667	0.634	0.94	0.89	1.05
	10.0 to 5.0	0.030	0.019	0.030	0.63	1.00	0.63
	5.0 to 1.2	0.255	0.238	0.272	0.93	1.07	0.86
Tungsten	15.0 to 10.0	0.682	0.684	0.670	1.00	0.98	1.02
	10.0 to 5.0	0.028	0.028	0.027	0.99	0.97	1.02
	5.0 to 1.2	0.256	0.181	0.241	0.71	0.94	0.76
Gold	15.0 to 10.0	0.405	0.278	0.406	0.69	1.00	0.69
	10.0 to 5.0	0.035	0.040	0.036	1.14	0.98	1.16
	5.0 to 1.2	0.359	0.279	0.335	0.78	0.93	0.84
Lead	15.0 to 10.0	0.668	0.667	0.658	1.00	0.98	1.02
	10.0 to 5.0	0.034	0.037	0.040	1.10	1.19	0.92
	5.0 to 1.2	0.414	0.328	0.437	0.79	1.06	0.75
²³² Th	15.0 to 10.0	0.650	0.667	0.661	1.03	1.02	1.01
	10.0 to 5.0	0.041	0.036	0.039	0.88	0.95	0.92
	5.0 to 1.2	0.342	0.336	0.324	0.98	0.95	1.04
²³⁸ U	15.0 to 10.0	0.658	0.683	0.674	1.04	1.03	1.01
	10.0 to 5.0	0.059	0.030	0.055	0.51	0.93	0.55
	5.0 to 1.2	0.506	0.390	0.489	0.77	0.97	0.78

*In counts per source neutron count.

^aExperiment.^bENDF/B-V.^cENDL.

TABLE III
 $\Sigma n_i C_i$ for Recoil Electrons

Material	$\Sigma n_i C_i \times 10^{-7}$			C/E		C_1/C_2
	C_2^a	C_1^b	E^c	C_2/E	C_1/E	
Blank	0.21	0.19	0.21	1.00	0.90	0.91
Carbon	0.85	0.75	1.02	0.91	0.83	0.91
Nitrogen	1.37	1.09	1.40	0.98	0.78	0.80
H ₂ O	1.04	0.74	0.94	1.15	0.82	0.72
CF ₂	1.15	0.75	0.84	1.37	0.89	0.65
Aluminum	2.08	1.56	2.00	1.08	0.81	0.75
Silicon	2.36	1.63	2.20	1.08	0.74	0.69
Titanium	1.60	1.86	2.05	0.78	0.91	1.16
Iron	1.59	1.23	1.61	1.09	0.84	0.77
Copper	1.69	1.83	1.72	0.98	1.06	1.08
Tantalum	1.09	0.94	1.20	0.91	0.78	0.86
Tungsten	0.69	0.69	0.85	0.82	0.82	1.00
Gold	0.51	0.51	0.53	0.96	0.96	1.00
Lead	0.75	0.58	0.63	1.19	0.93	0.78
²³² Th	0.71	0.63	0.72	0.98	0.88	0.90
²³⁸ U	0.83	0.72	0.82	1.02	0.88	0.87

^aENDL.^bENDF/B-V.^cExperiment.

tungsten target backing accounting for 26%, the remaining target structure accounting for 28%, and 46% generated in the air. The air-related gamma rays can be discounted because only a small fraction of these can pass through the collimator. Therefore, the source structure generates 54% (0.15 MeV), and 7% of this (0.01 MeV) may be attributed to stray deuteron beam effects upstream of the tritium target. When compared to strong gamma-ray converters such as silicon, which generates $\sim 2 \gamma$ MeV/n, we judge the upstream effects to be negligible.

Carbon

Figure 5 shows the measured neutron TOF and ERS spectra from a graphite sphere used in earlier studies.¹³ The overall agreement found for the TOF spectra is quite good, especially for the high-energy interval. However, ENDF/B-V underestimates the medium-energy interval by 17%, and ENDL underestimates the low-energy interval by 24%.

The self-indicating nature of the ERS caused by the prominent role of the 4.439-MeV excitation gamma ray provided an opportunity to correct the linearity relationship. Using the Compton edge from this gamma ray, we found that a value of 0.0110 for the constant c_2 in Eq. (3) gives a better fit to the channel number/electron energy relation.

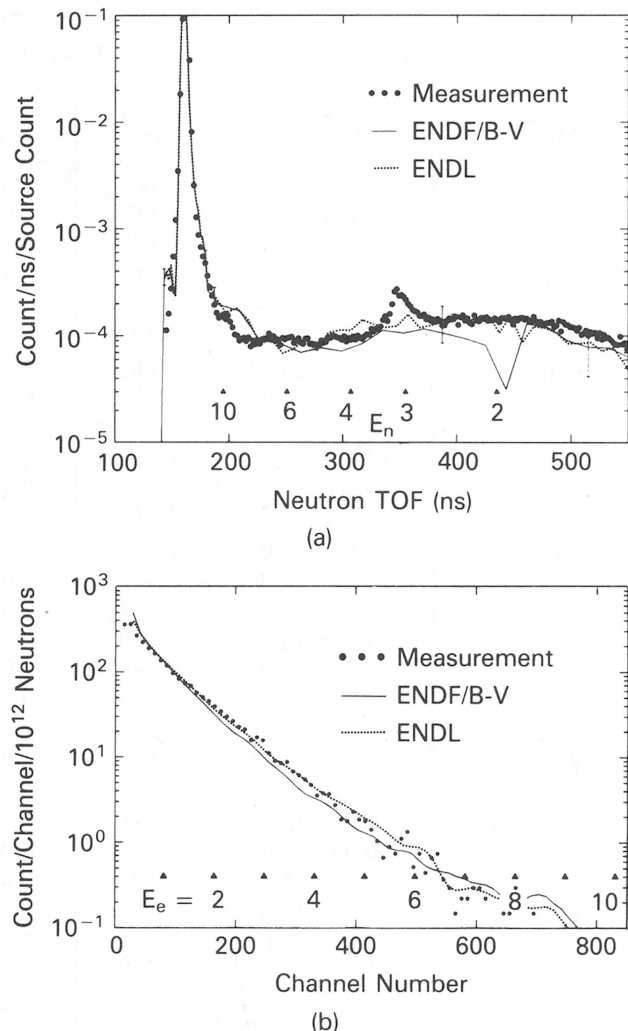
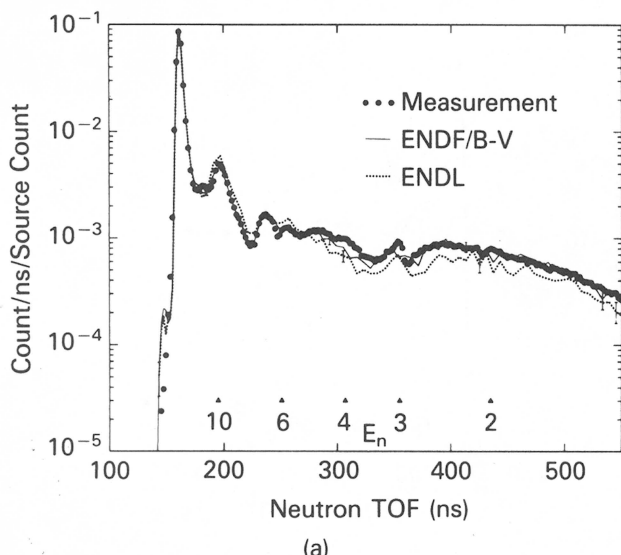


Fig. 4. Comparison of measured and calculated spectra from a blank run (no spherical assembly in place): (a) neutron TOF spectra and (b) ERS.

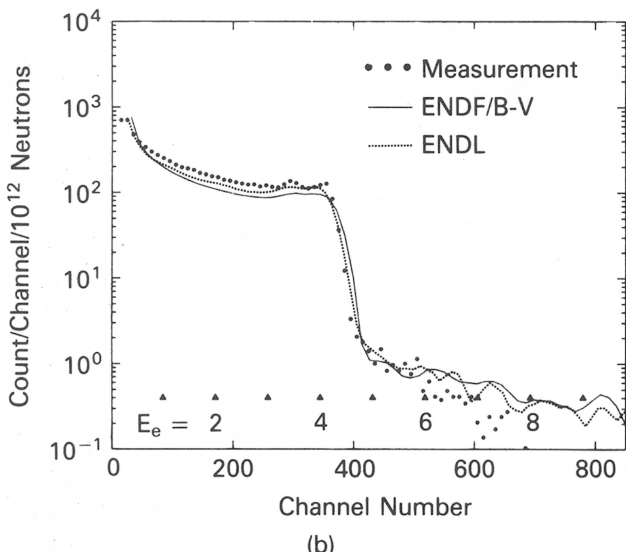
The C/E ratios in Table III seem to indicate that the inelastic neutron cross section to the 4.439-MeV level could be underestimated in the libraries by as much as 17% (ENDF/B-V). However, the good agreement found with the neutron TOF spectra does not support this conclusion. The present values for the $\sigma(n, n')$ to the 4.439-MeV level in carbon for 14-MeV neutrons are 231 mb in ENDL and 189 mb in ENDF/B-V. Taking into account the errors in the measurements (listed in Table IV), the differences between the neutron and gamma spectra comparisons may manifest, in large measure, accumulated uncertainties.

Nitrogen

The neutron and gamma measurements from nitrogen are displayed in Fig. 6. The agreement of these



(a)

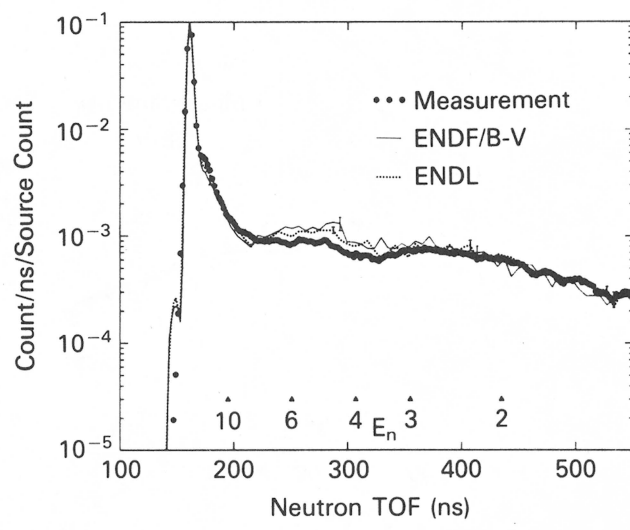


(b)

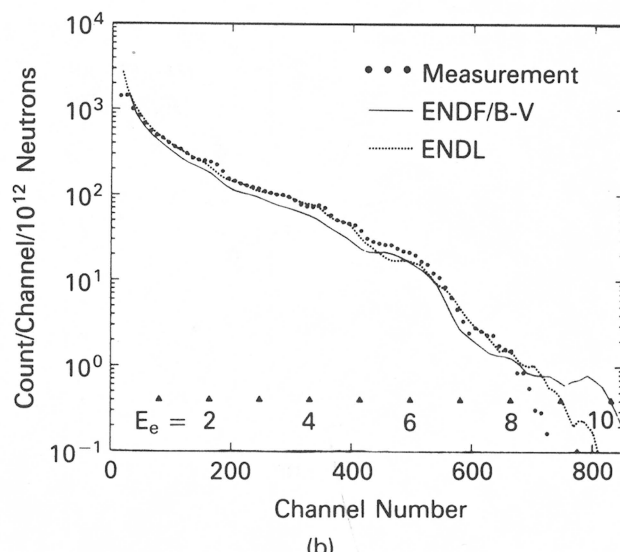
Fig. 5. Comparison of measured and calculated spectra from a spherical graphite assembly: (a) neutron TOF spectra and (b) ERS.

measurements with the calculated neutron TOF spectra is fairly good, although both libraries overestimate the production of neutrons in the medium-energy interval by $\sim 10\%$.

We first studied gamma rays from liquid nitrogen-filled spherical vessels⁶ in 1977. We wrote a Monte Carlo program, TORTEEP, to explicitly model the recoil electrons in the NE-213 detector. Because this early calculation did not allow for large-angle scattering of the electrons in the detector, we decided to repeat these calculations with SANDYL, as well as the measurements. The ENDF/B-V calculation underestimates the measurement by $\sim 20\%$, but both libraries agree with the measured (n, n') emission spectrum. This indicates that the contribution to the gamma-ray production



(a)



(b)

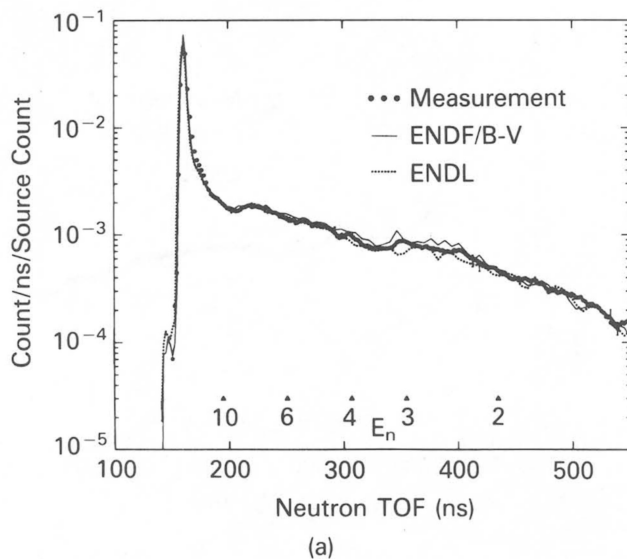
Fig. 6. Comparison of measured and calculated spectra from a spherical liquid nitrogen dewar vessel: (a) neutron TOF spectra and (b) ERS.

from $(n, \text{charged particle})$ cross sections in ENDF/B-V is lower than the ENDL data set. The ERS calculations based on ENDL agree closely with the measurements.

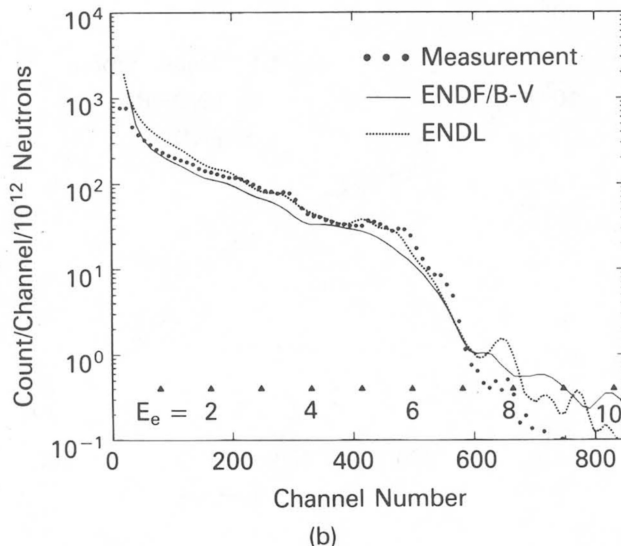
Water (H_2O)

In Fig. 7a, the measured neutron leakage spectrum from water was closely reproduced by the calculations, which tells us that the elastic and inelastic cross sections for ^{16}O are well represented in both libraries and have close to the same values.^{3,4} This agreement is the result of an earlier pulsed-sphere measurement¹⁴ for ^{16}O . The C/E ratios are about unity for the three neutron energy ranges.

The ERS from water (Fig. 7b) shows the signatures



(a)

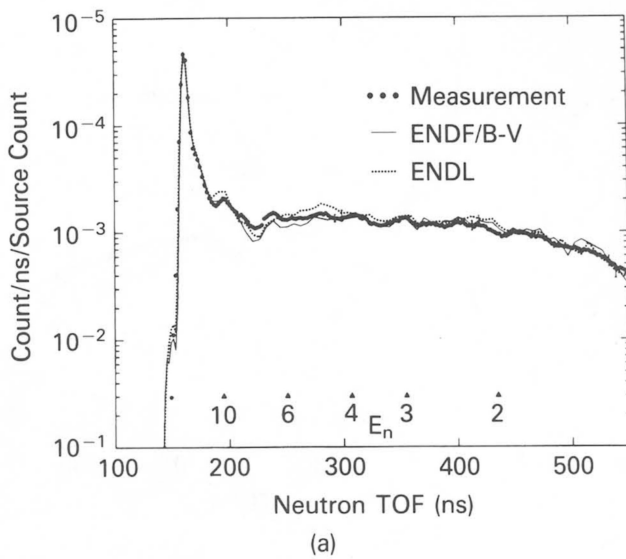


(b)

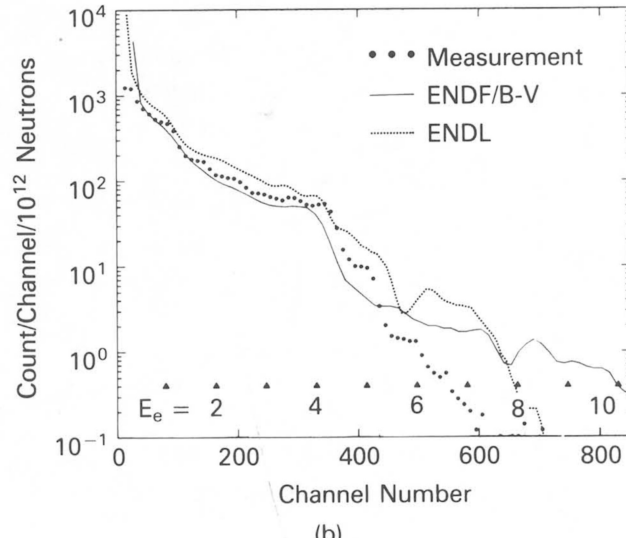
Fig. 7. Comparison of measured and calculated spectra from a water-filled spherical glass flask: (a) neutron TOF spectra and (b) ERS.

of the Compton edges from gamma rays emitted in the $^{16}\text{O}(n, n')$ reaction: $E_e = 6.7$ MeV from the 6.916 (2+)- and 7.117 (1-)-MeV levels, and $E_e = 5.9$ MeV from the 6.131 (3-)-MeV level. At $E_e = \sim 3.5$, the Compton edges from the 3.68- and 3.85-MeV gamma rays come from the (n, α) reaction.

The ENDL calculation agrees fairly well with the measured ERS, although improvements are needed, mainly for $E_e < 1.5$ MeV. The agreement shown was obtained only after a revision of the $(n, x\gamma)$ cross sections in the ENDL library. Our first comparison of the calculated ERS using this library and the measurements showed large discrepancies that were traced to an earlier input error in the $^{16}\text{O}(n, \alpha)$ cross sections in the ENDL data base. This correction, together with the in-



(a)



(b)

Fig. 8. Comparison of measured and calculated spectra from a spherical Teflon assembly: (a) neutron TOF spectra and (b) ERS.

clusion of the recent $(n, x\alpha)$ cross-section data of Kneff et al.¹⁵ resulted in the improved results shown in Fig. 7b. Details of the evolution of the ^{16}O cross sections are discussed elsewhere.¹⁶ The ENDF/B-V calculation is lower than the measurements by as much as 20%.

Teflon (C_2F_4)

To study fluorine, we used a Teflon (C_2F_4) spherical assembly. In Fig. 8b, both calculations agreed with the neutron TOF spectrum very well, with the ENDL slightly overpredicting the neutron peak around 10 MeV, as was the case for the 4.439-MeV level in carbon (Fig. 5a). The integrals of the neutron counts per

source neutron count are close to unity for all the energy intervals, with the exception of that calculated with the ENDF/B-V cross sections for the medium-energy interval, which is 14% lower than the measurements.

Our initial comparison of the ENDL-based ERS to the experimental ERS was very disappointing, with a C/E ratio $>4!$ We reevaluated the ^{19}F cross sections, including the $(n, x\alpha)$ results of Kneff et al.¹⁵ Figure 8b shows that the revised ENDL base is consistently higher than the experiment; the ENDF/B-V data set gives better agreement.

These results, as well as those for oxygen, show the value of a parallel analysis of the neutron and gamma-ray measurements. Where the excitation of the target nucleus is sufficiently high to permit the opening of decay channels that compete strongly with inelastic neutron scattering through charged-particle emission, the gamma-ray emission can be strongly suppressed.

Aluminum

The neutron TOF emission spectrum from aluminum was studied earlier¹⁷ as a function of mean-free-path for 14-MeV neutrons. For the present measurements, we found both libraries to be in excellent agreement with the calculated spectra, as shown in Fig. 9a and Table II. The ENDL cross sections fit the measured ERS well, while the ENDF/B-V calculation underestimates it.

Silicon

These are the first measurements for silicon under the pulsed-sphere program and, consequently, also a first test of the ENDL data base for this material. In Fig. 10a, we see that neither library reproduces the measured TOF spectrum well. The ENDL-based calculation results in an excess of preequilibrium neutrons (i.e., 8 to 12 MeV) and a dearth of neutrons at lower energies (8 to 2 MeV). The ENDF/B-V calculation agrees better with the experiment down to 8 MeV, underestimates the emission between 9 and 5 MeV by ~35%, and accurately reproduces the spectrum below 5 MeV.

The comparison of the experimental and calculated ERS spectra for silicon is shown in Fig. 10b. The ENDL calculation reproduces the features of the measured spectrum better up to ~5-MeV gammas, while the ENDF/B-V-based calculation is consistently lower. Accordingly, the silicon libraries in ENDL and ENDF/B-V need to be examined.

Titanium

In Fig. 11a, we see that neither library agrees closely with the measured TOF spectrum, which also was studied earlier.¹⁷ The preequilibrium neutrons are not well modeled, and they underestimate the produc-

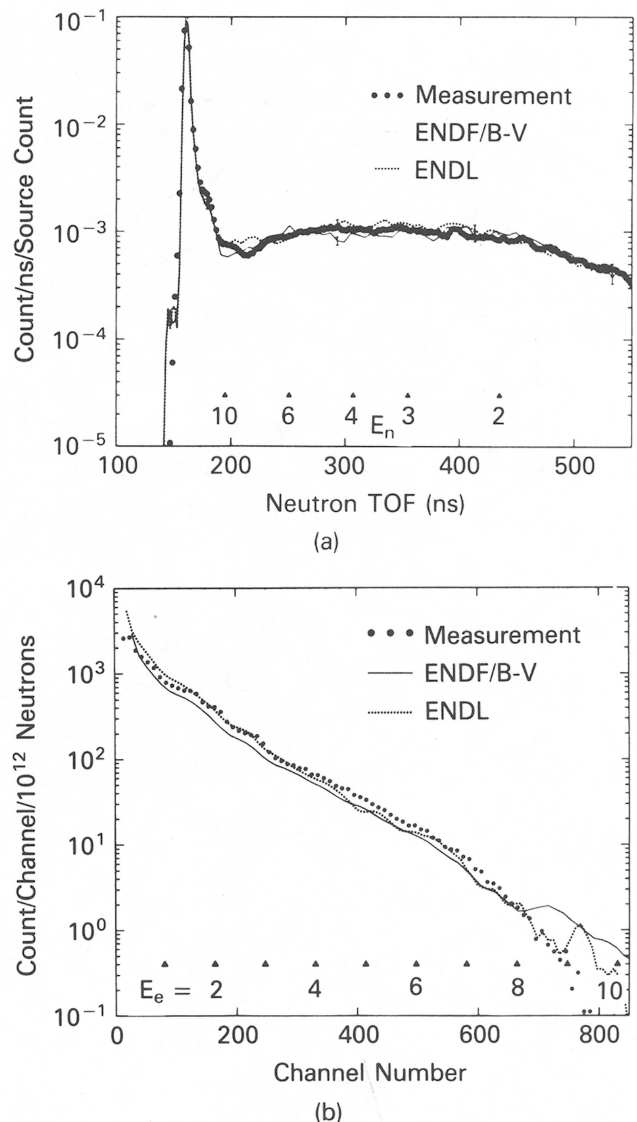


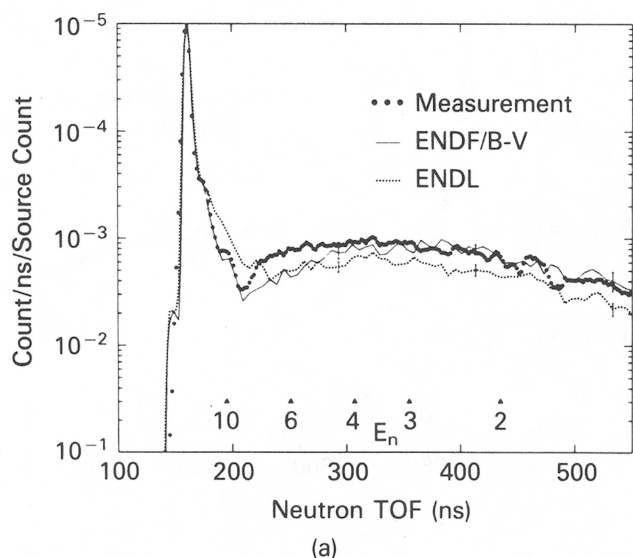
Fig. 9. Comparison of measured and calculated spectra from a spherical aluminum assembly: (a) neutron TOF spectra and (b) ERS.

tion of neutrons between 5 and 2.5 MeV, especially in the ENDF/B-V calculation.

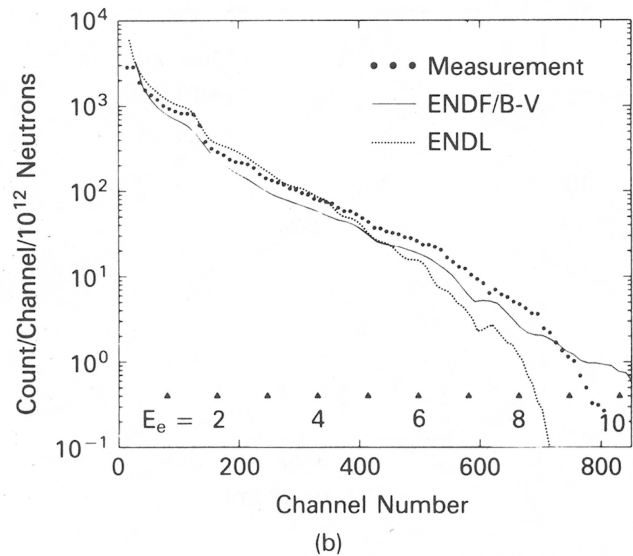
Figure 11b shows that the shape of the measured ERS is reproduced better by the ENDL data base over the whole energy range. However, the agreement of ENDL with experiment below $E_e = 2$ MeV is poorer than the ENDF/B-V comparison, leading to a lower C/E ratio for ENDL. The discrepancies are sufficiently large to justify a review of the two data bases.

Iron

Results of the pulsed-sphere studies of neutron transport through iron have been documented,¹⁸ and



(a)



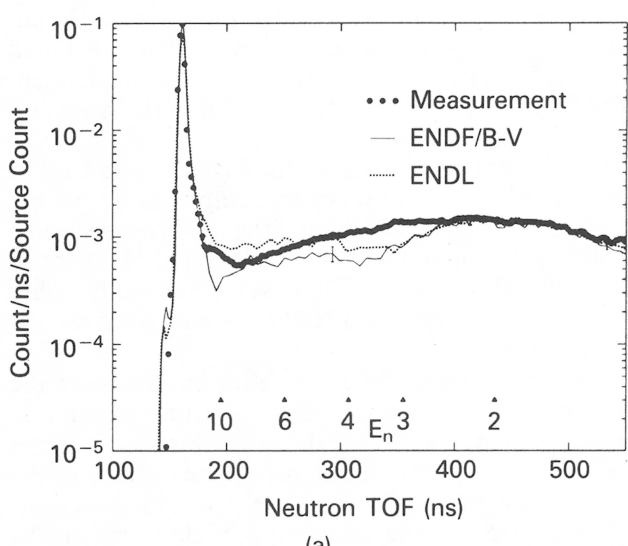
(b)

Fig. 10. Comparison of measured and calculated spectra from a spherical silicon assembly: (a) neutron TOF spectra and (b) ERS.

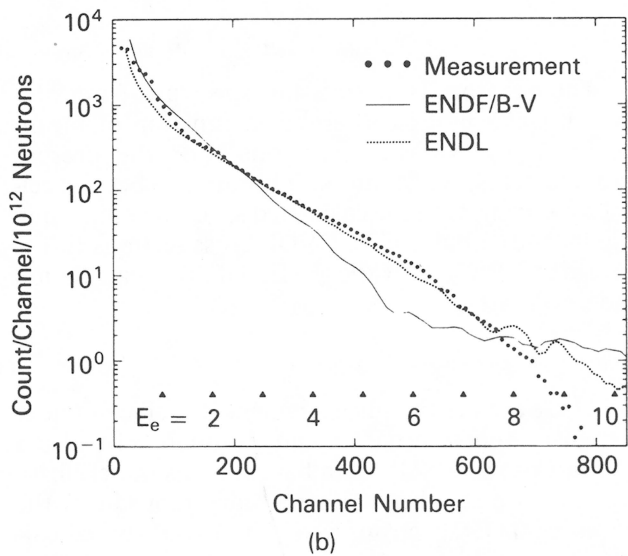
the current measurements of the neutron TOF spectrum shown in Fig. 12a agree very well with the published results and with both calculations. The ERS calculated with the ENDL cross sections is in very good agreement with the measurements (Fig. 12b), while ENDF/B-V underestimates it.

Copper

Application of the ENDL cross sections for copper leads to a very good agreement with the neutron TOF spectrum shown in Fig. 13a, while the calculation with the ENDF/B-V library completely lacks the emission of preequilibrium neutrons, as was shown in earlier studies.¹⁹ Except for the medium- and low-energy in-



(a)



(b)

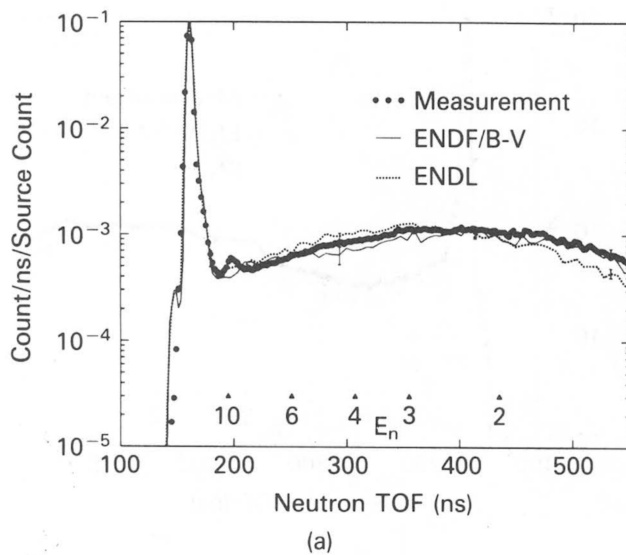
Fig. 11. Comparison of measured and calculated spectra from a spherical titanium assembly: (a) neutron TOF spectra and (b) ERS.

tervals, the C/E ratios obtained from the ENDF/B-V calculation are close to unity.

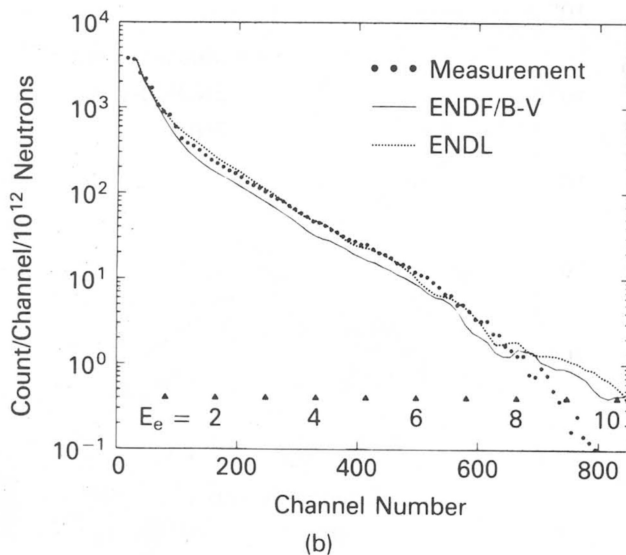
Both calculations fit the measured ERS (Fig. 13b) reasonably well, with ENDF/B-V giving a surprisingly better agreement than the ENDL calculation in spite of the poor results obtained for the neutrons. This inconsistency may result from independent neutron and gamma evaluations in the ENDF/B-V library, without the required energy conservation.

Tantalum

As seen in Fig. 14a, the calculated neutron emission spectra with ENDL and ENDF/B-V libraries agree rather well with the measured TOF spectrum, although



(a)

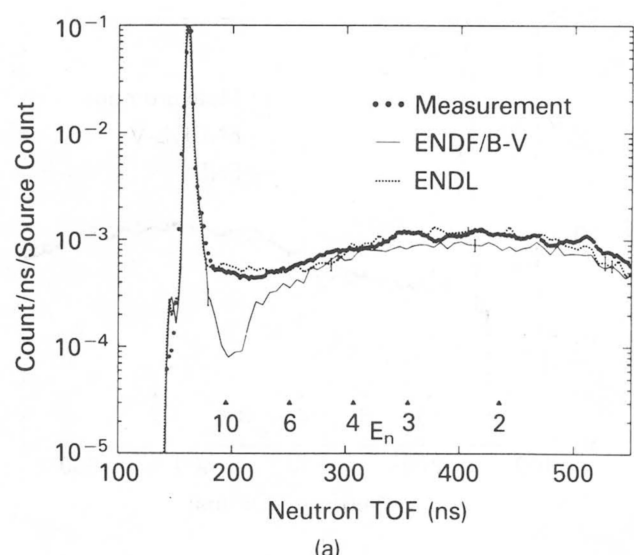


(b)

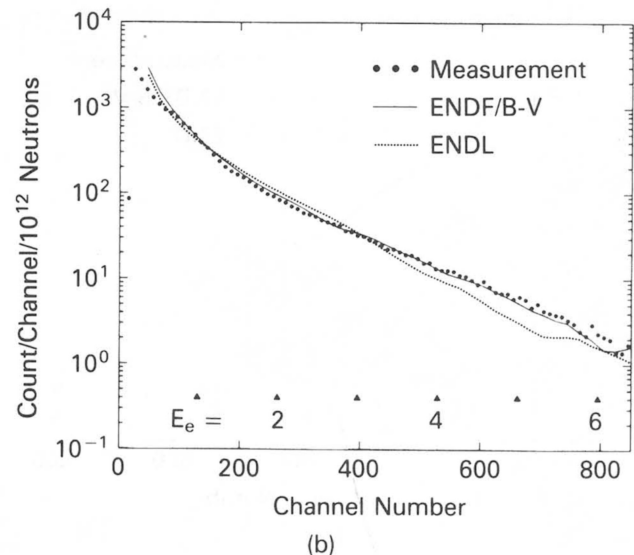
Fig. 12. Comparison of measured and calculated spectra from a spherical iron assembly: (a) neutron TOF spectra and (b) ERS.

there is a difference between the ENDF/B-V spectra in our work and those reported in Ref. 20. We believe the difference to be the result of a problem with the representation of the data we received in the ENDF/C format or with the code that translated the data from ENDF/C format to ENDL format.

The calculations agree with the measured ERS better for gamma energies below 3 MeV (Fig. 14b), but they both underestimate it at higher energies. Table III shows the ENDF/B-V calculation for $\Sigma n_i C_i$ to be 14% below that based on ENDL, which itself was 9% below experiment.



(a)



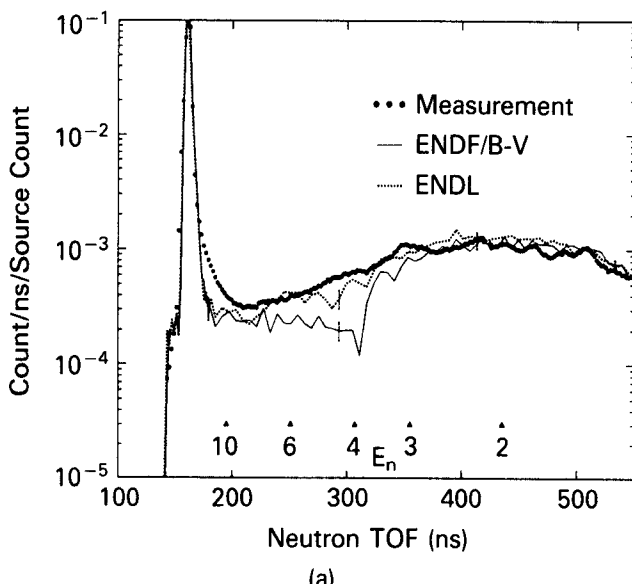
(b)

Fig. 13. Comparison of measured and calculated spectra from a spherical copper assembly: (a) neutron TOF spectra and (b) ERS.

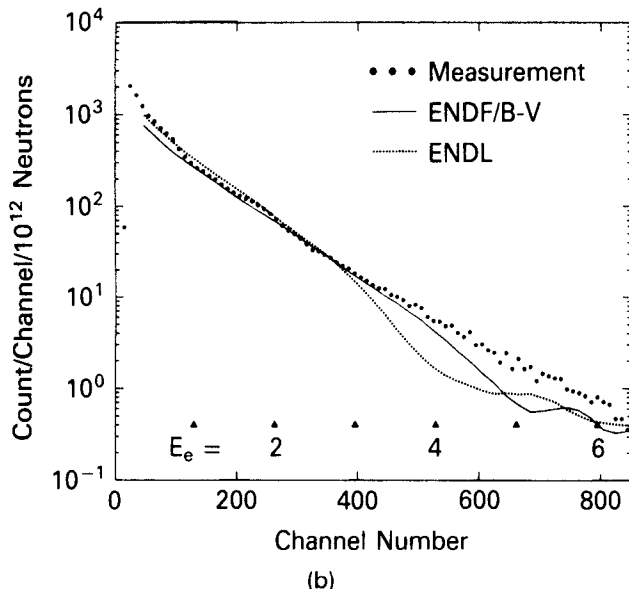
Tungsten

While both calculations fit the neutron TOF spectrum (Fig. 15a and Table II) reasonably well, ENDF/B-V underestimates the low-energy interval by ~30%.

The comparison of the measured and calculated ERS is shown in Fig. 15b. We obtained the improved agreement between the ENDL calculation and experiment after reevaluating the gamma production cross sections in this library. In the initial comparison, the ENDL calculation was 40% below the measured ERS. The comparison shown here gives $C/E = 0.82$ for both



(a)

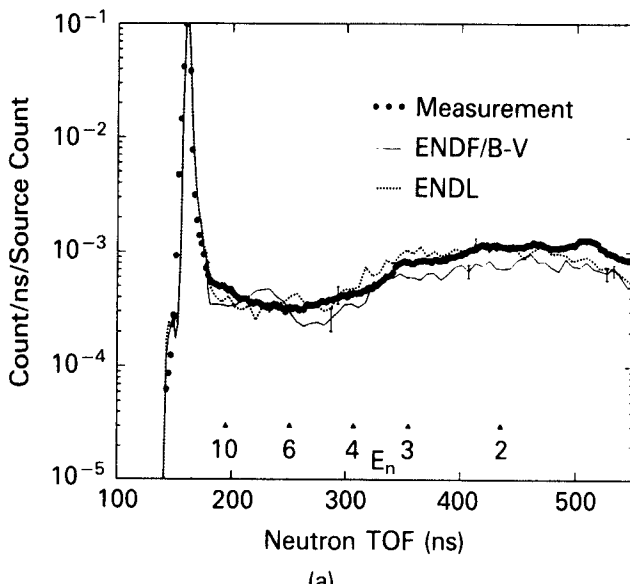


(b)

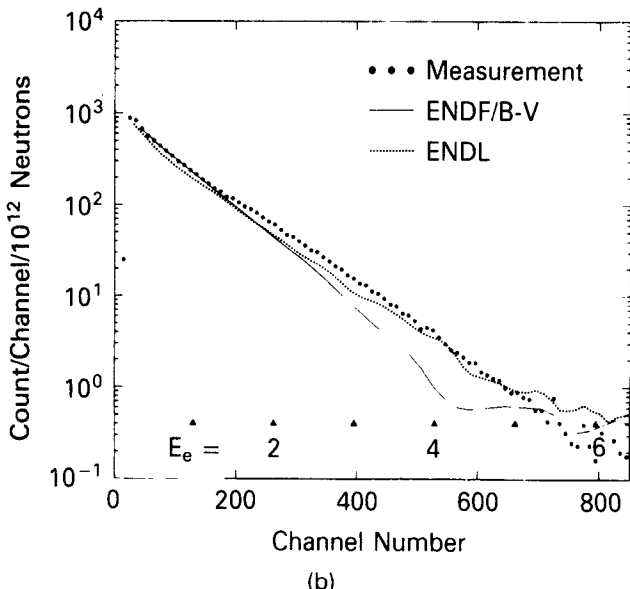
Fig. 14. Comparison of measured and calculated spectra from a spherical tantalum assembly: (a) neutron TOF spectra and (b) ERS.

ENDL and ENDF/B-V. The latter does very well for the low electron recoil energies.

We saw earlier, in the discussion of the blank run, that the tungsten backing, according to TART, contributed 26% of the generated gamma rays; i.e., 0.07 MeV. Applying the above C/E ratio to this value yields a 0.013-MeV underestimation of gamma-ray energy from the backing on the tungsten sample. Its contribution to the gamma-ray leakage is further suppressed by the shielding action of the spherical assembly in position. Consequently, we did not apply a correction for the tungsten backing in the other assemblies.



(a)



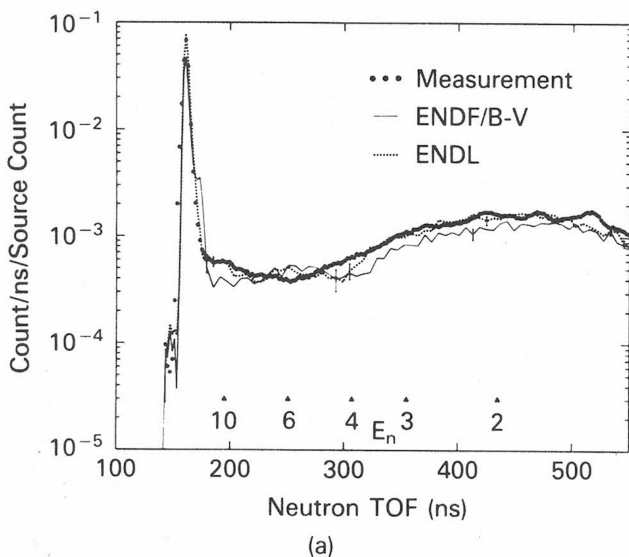
(b)

Fig. 15. Comparison of measured and calculated spectra from a spherical tungsten assembly: (a) neutron TOF spectra and (b) ERS.

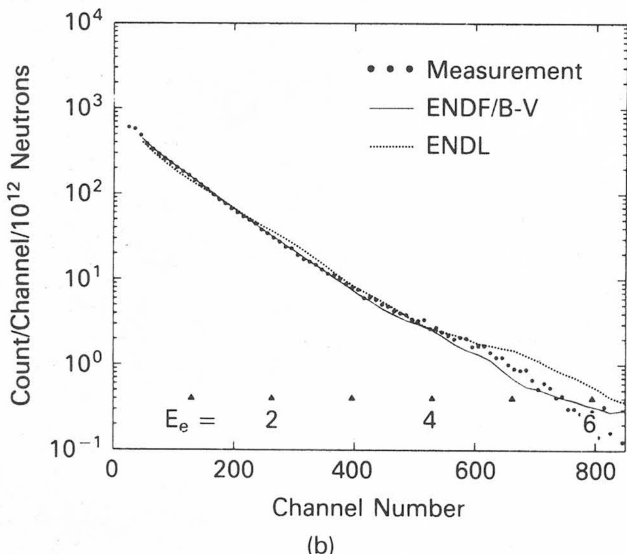
Gold

The calculation based on the gold data file in the ENDL library agrees very well with the measured TOF spectrum (Fig. 16a). In Table II, we see that the ENDF/B-V calculation is almost 30% low in the high-energy interval and 20% low for the low-energy interval.

The measured and calculated ERS are shown in Fig. 16b. Because ENDF/B-V does not have a gamma file for gold, the calculations were done with Los Alamos National Laboratory (LANL) T-2 cross sections.²¹ Both calculations agree with the experimental results.



(a)



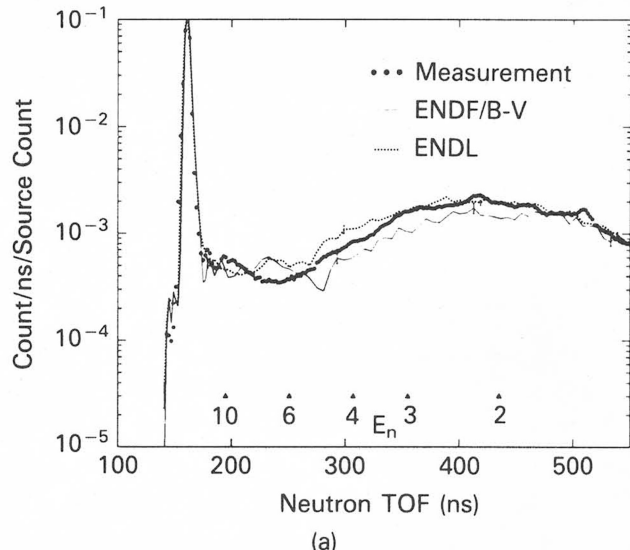
(b)

Fig. 16. Comparison of measured and calculated spectra from a spherical gold assembly: (a) neutron TOF spectra and (b) ERS.

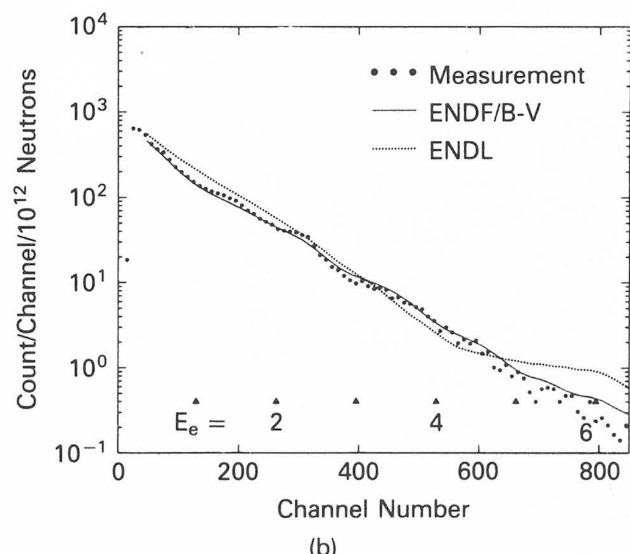
Lead

The lead neutron emission spectrum was studied earlier.²⁰ The present measurements and calculations shown in Fig. 17a do not agree with the results from the earlier ENDL calculation, which was done with a version of the ENDL data file in which the estimates were based on systematics for the secondary spectra of inelastically scattered neutrons. Subsequently, the estimates were replaced by model calculations for these spectra. ENDF/B-V underestimates the neutron production in the low-energy interval by 20%, with an overall good agreement with the measured TOF spectrum at higher energies.

The ERS calculated with ENDF/B-V is in excellent



(a)



(b)

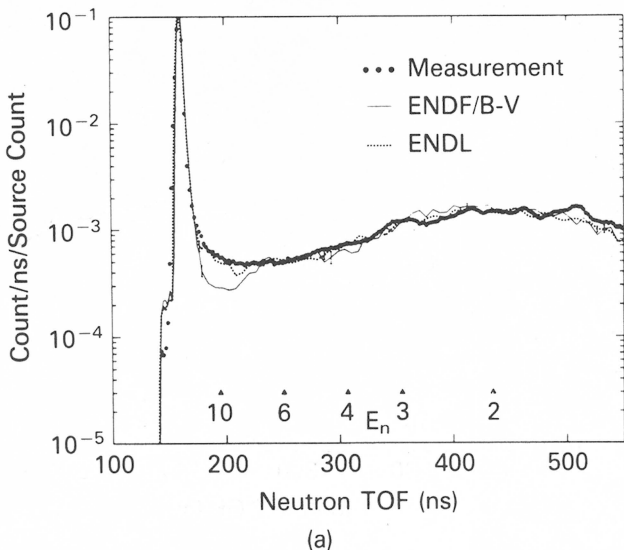
Fig. 17. Comparison of measured and calculated spectra from a spherical lead assembly: (a) neutron TOF spectra and (b) ERS.

agreement (Fig. 17b) with the measurements, while ENDL overestimates the experiment by ~20%.

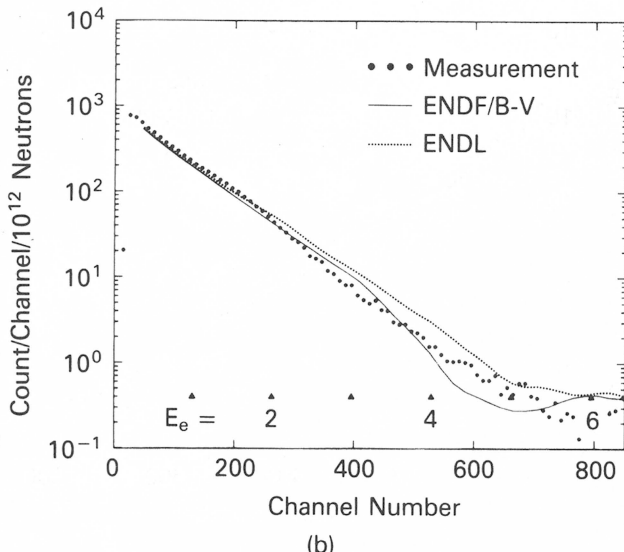
Thorium

The measured and calculated neutron TOFs from ²³²Th shown in Fig. 18a are in very good agreement with earlier comparisons.^{7,19} The ENDL cross-section set gives excellent agreement with the measurements for the whole neutron energy range. The ENDF/B-V calculation gives too few neutrons between 12 and 8 MeV.

The comparison of the ENDF/B-V set in Fig. 18b with the shape of the measured ERS is relatively good. Although ENDL overestimates the gamma-ray



(a)



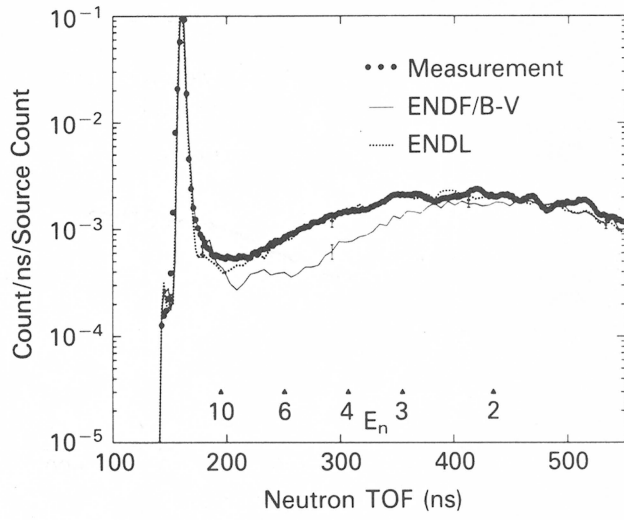
(b)

Fig. 18. Comparison of measured and calculated spectra from a spherical ^{232}Th assembly: (a) neutron TOF spectra and (b) ERS.

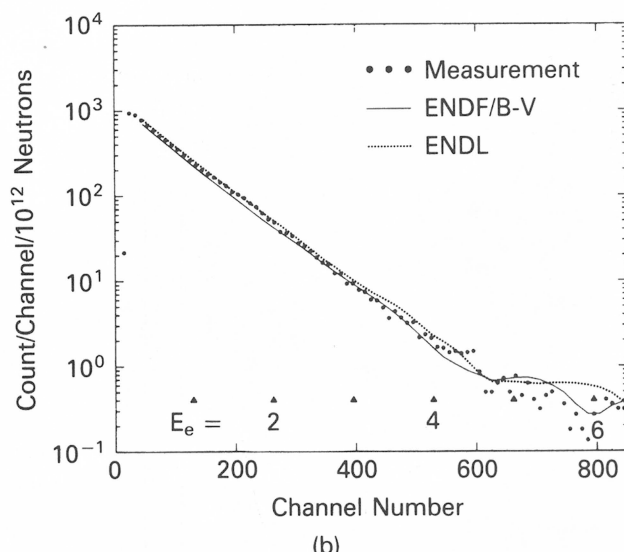
production above 2 MeV, it is closer to the experimental ERS below 2 MeV.

Uranium

Figure 19a shows the results obtained for the neutron emission from ^{238}U , which was also studied earlier.^{7,19} The ENDL library gives very good agreement with the present measurements, as it does in the ^{232}Th results. The ENDF/B-V cross sections underpredict the neutron emission in the medium-energy interval by almost 50% and in the low-energy interval by 20%. Both calculations fit the measured ERS well.



(a)



(b)

Fig. 19. Comparison of measured and calculated spectra from a spherical ^{238}U assembly: (a) neutron TOF spectra and (b) ERS.

ERROR ANALYSIS FOR THE ERS

In the present work, we have compared experimental pulse-height distributions, neutron TOF spectra, and ERS with their calculated counterparts. The TART code generates the neutron and gamma spectra, and SANDYL calculates the ERS generated by the gamma rays impinging on the detector. Because we have previously discussed in detail the error analysis for the neutron spectra,⁵ we limit our analysis here to the ERS. The calculated ERS are obtained in units of electron counts per channel per source neutron. We first discuss the different contributions to the error assigned to the measurements and calculations.

Neutron Source Calibration

To the absolute calibration of the neutron source obtained from the proton recoil counter and the alpha counter, we have assigned a $\pm 6\%$ uncertainty, based primarily on our confidence in the behavior of the proton recoil counter. In a typical run, the number of counts in these detectors were $>10^5$, which gives a statistical uncertainty $<1\%$.

Neutron Source Angular Distribution

The uncertainty in the angular distribution of the 14-MeV neutron source is estimated to be $\pm 1\%$ from calculation¹² and from our earlier work.⁸ The errors from calibration and angular distribution of the neutron source contribute to the error assigned to the strength of the neutron source.

Room Background

The shadow-shield experiment discussed earlier showed the contribution from the room background to be 7% of the ERS measured for a typical blank run. As already discussed, the blank run gave $\sim 0.15 \gamma/\text{MeV}$ per 14-MeV neutron, and 7% of that amounts of $0.01 \gamma/\text{MeV}/\text{n}$, originating most likely in the beam transport pipes upstream of the tritium target visible to the NE-213 detector. For example, in the iron sphere measurements, we found a gamma-ray output of $\sim 1.4 \gamma/\text{MeV}/\text{n}$. If we assume that $0.01 \gamma/\text{MeV}/\text{n}$ comes from the room background, this results in a 0.7% contribution.

We approximated the presence of air in the experimental setup by assuming a spherical zone of radius D (source-detector distance). The thickness of this air zone was $\rho \approx 1.1 \text{ g/cm}^2$, resulting in a 3% attenuation of the gamma rays. Furthermore, our calculational model included an edit procedure to filter out gamma rays coming into the collimator at larger angles than the one defined by the diameter and position of the collimator and the detector position. The uncertainty is estimated to be 1%.

Another subtle component of the room background is the electrons, generated by gamma rays in the air and collimator surfaces, that impinge directly on the detector face. This effect was studied by performing SANDYL calculations with a simplified geometry and source description. We found that the contribution of these background electrons (coming mainly from the inner collimator surface) to the measured ERS was $\leq 1\%$.

The contribution of the room background, target assembly, and collimators to the measured neutron emission spectra is discussed in detail in Ref. 8.

Characteristics of the Spherical Assembly

The uncertainty in the value of $\rho\Delta R$ is estimated to be 1%. Since we chose ρR to maximize the leakage of

gamma rays, the effect of a 1% error in $\rho\Delta R$ is negligible.

Placement of Neutron Source Target

The position of the tritium target (mounted at the end of the low-mass assembly) at the center of the sphere is estimated to be accurate within $\pm 0.1 \text{ cm}$. The TART calculations showed that a displacement of $\pm 0.1 \text{ cm}$ in the neutron source position generally results in a $\pm 2\%$ change in the gamma-ray energy fluence.

Location of the Detector

The distance between the neutron source and center of the NE-213 detector was 852.5 cm , with an uncertainty of $<1 \text{ cm}$. This contributes $\sim 0.2\%$ to the overall uncertainty.

Modeling and Calibration of Detector

We x-rayed the NE-213 detector to check the dimensions against the manufacturer's specifications, and we found serious discrepancies. The gas bubble that occupied $\sim 6\%$ of the enclosed cylindrical space was represented as an annular bubble at the outer portion of the liquid scintillator in order to simplify the calculations. The annulus degraded the energy deposited by the electrons by $\sim 7\%$. These details became irrelevant as a result of the calibration procedure of the detector. Recalling a correction factor of 1.05 for the first series of measurements and 1.10 for the second series, we conservatively estimate the statistical uncertainty assigned to the detector to be $\pm 5\%$.

A belated three-dimensional SANDYL calculation that included the true shape of the gas bubble in the detector resulted in a 6% energy degradation of the NE-213 detector sensitivity, thus confirming our initial estimate, within statistical significance.

Reproducibility of the Measurements

Common to both series of measurements were the spherical assemblies of graphite, aluminum, water, and iron. The average variation in the values of the C/E ratios obtained for these materials from the two sets of measurements was $\pm 5.4\%$. The largest difference between the two sets of values was for iron, where we found a $\pm 9\%$ variation.

Conversion Factor

The value of the conversion factor [see Eq. (1)], which allowed conversion of the SANDYL output to the measured spectrum (count/channel), was observed to change as much as $\pm 4\%$ during the two series of measurements. This estimate was obtained from the displacement of the Compton edge of the 4.439-MeV gamma ray from carbon (graphite and C_2F_4 spheres) and is attributed to a gain shift in the amplifier.

Pulse-Shape Discrimination

We stored the neutron and gamma-ray pulses from the NE-213 detector in separate analog-to-digital converters. By using pulse-shape discrimination, we had a very clean separation of the neutron- and gamma-induced counts. The overlap between neutrons and gammas was <1%.

Gamma-Ray Time Window

To reduce the room-return background in the ERS measurements, we imposed a 22-ns time window. The start time was determined, with no spherical assembly in place, to be 2 to 3 ns before the prompt gamma-ray peak. We estimate a <0.5% signal loss as a result of this time cutoff because the transit time for 14-MeV neutrons across the sphere is ~3 ns, even for the largest spherical assemblies employed in this study.

Statistics for TART and SANDYL

The TART calculations generated on the average $\sim 10^6$ neutrons and $>10^4$ gamma rays, which were tallied across a spherical surface within a 30-deg half-angle. In the SANDYL calculations, 4×10^5 gamma rays were followed with $\sim 10^5$ interacting in the NE-213 detector. Since we chose 100 bins to sort the electron deposition energy, the average population per bin was 10^3 counts. The statistics were poorer for higher electron energies.

Error Analysis Summary

Table IV summarizes the assignments. After adding by quadrature, we assign $\pm 9\%$ to the calculated

ERS and $\pm 6\%$ to the measured ERS, in addition to statistics.

In many of the preceding ERS comparisons, we observed large differences between the ERS curves based on ENDL and ENDF/B-V. It is quite reasonable, therefore, to attribute errors to these data bases that would significantly affect the ERS calculations, especially when the differences between two sets of ERSs exceed the cumulative uncertainties derived above. We do not feel justified in selectively adjusting individual cross sections to bring about agreement between the measurements and calculations; therefore, many discrepancies remain. On the other hand, as we show next, we have used the measured $\Sigma n_i C_i$ to scale $(\sigma E)_\gamma$, the gamma-ray energy weighted gamma-ray production cross section.

DISCUSSION

If one is interested in gamma-ray energy production, a useful quantity to calculate is given by

$$(\sigma E)_\gamma = \int E_\gamma \frac{d\sigma}{dE_\gamma} dE_\gamma , \quad (4)$$

where the cross section is a function of the gamma energy. Equation (4) conveys information on the "hardness" of the gamma-ray spectrum. Table V lists values of $(\sigma E)_\gamma$ measured in Refs. 22 through 39. The values from the ENDL (TL880401 and TG880420) and ENDF/B-V evaluations are also given in Table V. The final column gives an estimate of $(\sigma E)_\gamma$ at a neutron energy of 14 MeV inferred from the present set of pulsed-sphere measurements. The detector thresholds differ among the sets. Whereas the range is $0 \leq E_\gamma \leq 20$ MeV

TABLE IV
Sources of Uncertainty in Calculated and Experimental Recoil Electron Spectra

Number	Item	Systematic (%)	Statistical (%)
1	Neutron source calibration	6	1
2	Neutron source angle distribution	1	---
3	Room background	1	---
4	Sphere characterization	<1	---
5	Source target position	2	---
6	NE-213 detector position	<1	---
7	Bubble model, NE-213 calibration	5	---
8	Reproducibility of experiments	5	---
9	Conversion factor	4	---
10	Pulse-shape discrimination	<1	---
11	Gamma-ray time window	<1	---
12	TART/SANDYL statistic	---	<10
	Net (Nos. 1 and 2)	---	6 (measurement)
	Net (Nos. 3 through 11)	---	9 (calculation)

TABLE V
Values of $(\sigma E)_\gamma$ for $E_n = 14$ MeV

Material	$(\sigma E)_\gamma$ (b·MeV)						
	ENDL	ENDF/B-V	ORNL	Ref. 22	Ref. 23	Others	Present Experiment
Carbon	1.022	0.841	0.80 (Ref. 25)	---	1.13	---	1.07
^{14}N	2.286	1.851	1.8 (Ref. 26)	---	---	0.89 (Ref. 37)	2.35
^{16}O	3.062	2.298	2.5 (Ref. 27)	---	---	---	2.73
Fluoride	1.804	0.961	0.86 (Ref. 28)	---	---	0.63 (Ref. 37)	0.93
Aluminum	6.313	4.647	4.3 (Ref. 29)	4.1	5.7	---	5.80
Silicon	7.300	5.756	4.7 (Ref. 30)	4.7	7.2	4.30 (Ref. 38)	7.30
Titanium	6.681	8.111	8.4 (Ref. 31)	6.7	10.5	---	8.70
Iron	9.220	7.537	11.1 (Ref. 32)	6.8	10.2	---	8.70
Copper	6.009	7.664	5.9 (Ref. 33)	5.4	---	---	6.70
Tantalum	12.37	9.856	4.3 (Ref. 25)	10.2	15.6	4.60 (Ref. 39)	13.1
Tungsten	9.932	10.08	10.0 (Ref. 34)	---	16.0	---	12.2
Gold	8.686	---	8.9 (Ref. 35)	---	---	---	9.00
Lead	9.911	7.531	7.9 (Ref. 36)	---	11.1	---	8.20
^{232}Th	11.57	9.619	---	12.6	---	---	11.9
^{238}U	13.92	12.60	---	12.9	19.3	---	14.0

for the evaluations, it is $0.3 \leq E_\gamma \leq 8.5$ MeV for Ref. 22, $0.5 \leq E_\gamma \leq 12.0$ MeV for Ref. 23, and 0.3 to $1.6 \leq E_\gamma \leq 10.5$ MeV for the Oak Ridge National Laboratory (ORNL) work.²⁴⁻³⁶

For some of the materials, the spread in the listed values beyond their quoted errors indicates that there are major discrepancies among the data. Sugiyama, in an earlier and more extensive review,⁴⁰ observed the considerable spread in $\sigma(n, xy)$ values. A recent LANL measurement³⁹ for tantalum agrees with the earlier ORNL results,²⁵ but these two experiments yield $(\sigma E)_\gamma$ values less than half those reported in Refs. 22 and 23. Normalizing to a common gamma-ray threshold of 0.3 MeV and relying on Drake's spectral shape²² above 0.3 MeV and ENDL cross sections below 0.3 MeV, we find

1. ENDL: 11.8 b·MeV
2. ENDF/B-V: 9.5 b·MeV
3. Ref. 22: 10.2 b·MeV
4. Ref. 23: 16.7 b·MeV
5. Ref. 25: 5.1 b·MeV
6. Ref. 39: 4.8 b·MeV
7. present series: 12.6 b·MeV.

To allow the users of neutron-photon computational models to test the validity of their models, we have generated a set of recommended values of $\gamma\text{MeV}/\text{n}$ based on our experimental results for the materials used in this study. These values were generated by performing

TART one-zone, one-dimensional, sphere calculations for each material. The calculations were done over a range of σR values to find the maximum gamma-ray leakage per 14-MeV neutron generated at the sphere center. The radius in each case was taken to be 1.0 cm, and each problem was run to a census time of 80 ns. Figure 20 illustrates the TART results for ^{14}N using the ENDL cross sections. We see that a maximum of $1.35 \gamma\text{MeV}/\text{n}$ escapes for $\sigma R = 40 \text{ g/cm}^2$. We corrected this value by dividing by C/E = 0.975 (given in Table III for ^{14}N calculated with ENDL) to give $1.38 \gamma\text{MeV}/\text{n}$. A similar procedure done with the ENDF/B-V nitrogen cross sections gave a calculated value of 1.14, corrected to $1.46 \gamma\text{MeV}/\text{n}$. Table VI gives the calculated and recommended values for the maximum $\gamma\text{MeV}/\text{n}$ for each material for the two libraries. The value of σR used in the calculations is given in the last column. For those materials where the difference in the recommended values among the two libraries is larger than the quoted errors (Table IV), we feel that the best value is that for which C/E (Table III) is closer to unity.

SUMMARY AND CONCLUSIONS

We have performed and analyzed a series of pulsed-sphere measurements designed to assess the predictive capability of the TART Monte Carlo neutron-photon transport code. This work focused on the leakage of gamma rays generated by 14-MeV neutrons, although the neutron emission spectra were measured simultaneously. We have not discussed the neutron results in detail because they were consistent with earlier

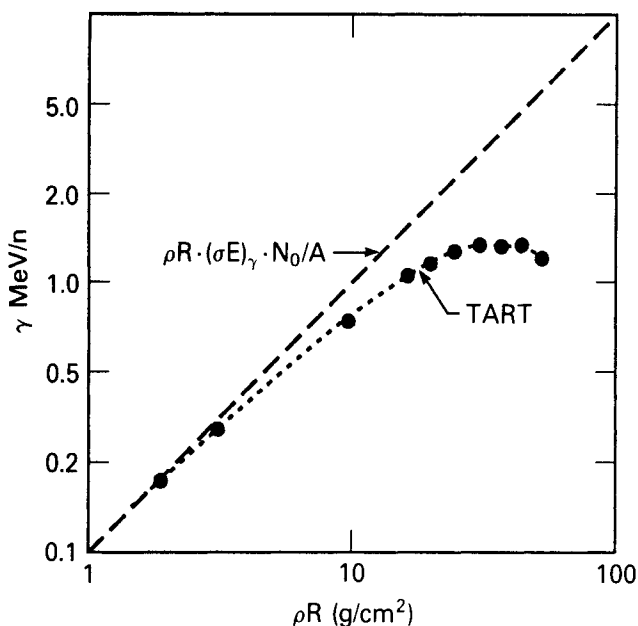


Fig. 20. Dependence of gamma-ray energy leaked from a uniform nitrogen sphere with a 14-MeV neutron source at its center, as a function of ρR .

work.⁵ In the calculations, we used two independent neutron cross-section data bases, LLNL's ENDL and the more widely distributed ENDF/B-V set.

We found the cross sections for ^{16}O and ^{19}F in the ENDL set to be deficient. We reevaluated them, incorporating more recent differential measurements.¹⁵ Furthermore, for oxygen, the comparison with the measurements uncovered an earlier error in the input

cross sections. The new calculation for water gave very good agreement with the measurements (Fig. 5b). For Teflon, improvements are still needed (Fig. 6b), although the new set succeeded in considerably reducing the initial discrepancies with the measurements.

To compare experimental and calculational results, we chose the quantity $\sum n_i C_i$ as a measure of the leakage of gamma-ray energy. The validity of this relation resulted from the gamma-ray calibration of the detector, which established that the energy deposited in the detector by the recoil electrons correlated linearly with channel number. We have compared the value of $\sum n_i C_i$ from the calculations obtained for each library with that from the experiment. Averaging over the 15 measurements, we found

1. $C/E = 1.02 \pm 0.15$ for ENDL
2. $C/E = 0.86 \pm 0.08$ for ENDF/B-V
3. $C_{\text{ENDF/B-V}}/C_{\text{ENDL}} = 0.86 \pm 0.15$.

In a review of the literature, we found generally poor agreement among measurements of the energy-weighted cross sections for gamma-ray production by 14-MeV neutrons, as illustrated in Table V. Recognizing that integral measurements do not allow extraction of microscopic cross sections, we have nevertheless estimated from the present data the values of $\sigma(n, x\gamma)E_\gamma$, scaling as $\sum n_i C_i$.

We have also used the TART code to generate leakage of gamma-ray energy, corrected according to the C/E ratio of $\sum n_i C_i$ found from the pulsed-sphere analysis. These uniform one-zone one-dimensional

TABLE VI
Gamma-Ray Mega-Electron-Volt per 14-MeV Neutron, Normalized to Pulsed-Sphere Experiments

Material	$(\gamma \text{ MeV/n})$		$(\gamma \text{ MeV/n})/(C/E)$		$(\rho R)_{\text{max } \gamma} \text{ (g/cm}^2)$
	ENDL	ENDF/B-V	ENDL	ENDF/B-V	
Carbon	0.90	0.85	0.99	1.03	40
Nitrogen	1.35	1.14	1.38	1.46	40
H_2O	0.93	0.71	0.81	0.87	25
C_2F_4	0.98	0.61	0.72	0.69	35
Aluminum	1.97	1.58	1.82	1.98	35
Silicon	2.15	1.67	2.00	2.26	35
Titanium	1.44	1.53	1.84	1.68	45
Iron	1.49	1.25	1.37	1.49	40
Copper	0.89	0.99	0.91	0.93	45
Tantalum	0.51	0.43	0.56	0.55	35
Tungsten	0.42	0.39	0.52	0.48	35
Gold	0.33	---	0.35	---	40
Lead	0.35	0.29	0.30	0.31	35
^{232}Th	0.34	0.29	0.35	0.34	35
^{238}U	0.38	0.32	0.37	0.38	35

spheres for 15 different materials may prove to be convenient benchmark exercises for users of coupled neutron/gamma-ray transport codes. The spheres had a $\rho R \approx 35 \text{ g/cm}^2$, where the maximum gamma-ray leakage generally occurs.

These results show the need for further accurate work in the field of gamma-ray production by 14-MeV neutrons.

REFERENCES

1. E. F. PLECHATY and J. R. KIMLINGER, "TARTNP: A Coupled Neutron-Photon Monte Carlo Transport Code," UCRL-50400, Vol. 14, Lawrence Livermore National Laboratory (1976).
2. H. M. COLBERT, "SANDYL, A Computer Program for Calculating Combined Photon-Electron Transport in Coupled Systems," SLL-74-0012, Sandia National Laboratories (1974).
3. "ENDL, Lawrence Livermore National Laboratory (LLNL) Evaluated Nuclear Data Library," UCRL-50400, Vol. 15, Parts A to E, Lawrence Livermore National Laboratory (1975-1978). The April 1, 1988 version of this library was used in the present study.
4. "ENDF/B Summary Documentation," ENDF-201, National Nuclear Data Center, Brookhaven National Laboratory (Sep. 1987).
5. L. F. HANSEN, E. GOLDBERG, R. J. HOWERTON, T. T. KOMOTO, and B. A. POHL, "Updated Summary of Measurements and Calculations of Neutron and Gamma-Ray Emission Spectra from Spheres Pulsed with 14-MeV Neutrons," UCID-19604, Rev. 1, Lawrence Livermore National Laboratory (1989).
6. L. F. HANSEN, T. T. KOMOTO, E. F. PLECHATY, B. A. POHL, G. S. SIDHU, and C. WONG, *Nucl. Sci. Eng.*, **62**, 550 (1977).
7. L. F. HANSEN, T. T. KOMOTO, E. F. PLECHATY, B. A. POHL, E. GOLDBERG, R. J. HOWERTON, and W. M. WEBSTER, *Nucl. Sci. Eng.*, **72**, 35 (1979).
8. C. WONG, J. D. ANDERSON, P. BROWN, L. F. HANSEN, J. L. KAMMERDIENER, C. M. LOGAN, and B. A. POHL, "Livermore Pulsed Sphere Program, Program Summary Through July 1971," UCRL-51144, Rev. 2, Lawrence Livermore National Laboratory (1972).
9. D. W. KNEFF, B. M. OLIVER, E. GOLDBERG, and R. C. HAIGHT, *Nucl. Sci. Eng.*, **94**, 136 (1986).
10. E. GOLDBERG, L. F. HANSEN, R. J. HOWERTON, T. T. KOMOTO, and B. A. POHL, "Hotspur: Neutron and Gamma Ray Emission from the Transport of 14-MeV Neutrons Through H_2O ," UCID-21064, Lawrence Livermore National Laboratory (1987).
11. J. H. THORNGATE, "Improvements in Apparatus and Procedures for Using an Organic Liquid Scintillator as a Fast-Neutron Spectrometer for Radiation Protection Applications," UCID-20664, Lawrence Livermore National Laboratory (1987).
12. J. D. SEAGRAVE, "D(D,n)³He and T(D,n)⁴He Neutron Source Handbook," LAMS-2162, Los Alamos National Laboratory (1958).
13. L. F. HANSEN, J. D. ANDERSON, E. GOLDBERG, E. F. PLECHATY, M. STELTS, and C. WONG, *Nucl. Sci. Eng.*, **35**, 227 (1969).
14. M. L. STELTS, J. D. ANDERSON, L. F. HANSEN, E. F. PLECHATY, and C. WONG, *Nucl. Sci. Eng.*, **46**, 53 (1971).
15. D. W. KNEFF, B. M. OLIVER, HARRY FARRAR IV, and L. R. GREENWOOD, *Nucl. Sci. Eng.*, **92**, 491 (1986).
16. E. GOLDBERG, L. F. HANSEN, R. J. HOWERTON, T. T. KOMOTO, and B. A. POHL, *Trans. Am. Nucl. Soc.*, **54**, 301 (1987).
17. L. F. HANSEN, S. M. GRIMES, R. J. HOWERTON, and J. D. ANDERSON, *Nucl. Sci. Eng.*, **61**, 201 (1976).
18. L. F. HANSEN, J. D. ANDERSON, R. J. HOWERTON, J. L. KAMMERDIENER, C. M. LOGAN, E. F. PLECHATY, and C. WONG, *Nucl. Sci. Eng.*, **51**, 278 (1973).
19. L. F. HANSEN, C. WONG, T. T. KOMOTO, B. A. POHL, and R. J. HOWERTON, *Nucl. Technol.*, **51**, 70 (1980).
20. L. F. HANSEN, H. M. BLANN, R. J. HOWERTON, T. T. KOMOTO, and B. A. POHL, *Nucl. Sci. Eng.*, **92**, 382 (1986).
21. P. G. YOUNG, Los Alamos National Laboratory, Private Communication (1988).
22. D. M. DRAKE, E. D. ARTHUR, and M. G. SILBERT, *Nucl. Sci. Eng.*, **65**, 49 (1978).
23. V. M. BEZOTOSNYI, V. M. GORBACHEV, M. S. SHVETSOV, and L. M. SUROV, *At. Energ.*, **49**, 239 (1980).
24. J. K. DICKENS, G. L. MORGAN, G. T. CHAPMAN, T. A. LOVE, E. NEWMAN, and F. G. PEREY, *Nucl. Sci. Eng.*, **62**, 515 (1977).
25. G. L. MORGAN, T. A. LOVE, J. K. DICKENS, and F. G. PEREY, "Gamma-Ray-Production Cross Sections of Tantalum and Carbon for Incident Neutron Energies Between 0.007 and 20.0 MeV," ORNL-TM-3702, Oak Ridge National Laboratory (1972).
26. J. K. DICKENS, T. A. LOVE, and G. L. MORGAN, "Gamma-Ray Production Due to Neutron Interactions with

- Nitrogen. . . ,” ORNL-4864, Oak Ridge National Laboratory (1973).
27. G. L. MORGAN and G. T. CHAPMAN, “The O($n, x\gamma$) Reaction Cross Section for Incident Neutron Energies Between 6.5 and 20.0 MeV,” ORNL-5575, Oak Ridge National Laboratory (1979).
 28. J. K. DICKENS, T. A. LOVE, and G. L. MORGAN, “Gamma Ray Production Due to Neutron Interactions with Fluorine and Lithium for Incident Neutron Energies Between 0.55 and 20 MeV,” ORNL-TM-4538, Oak Ridge National Laboratory (1974).
 29. J. K. DICKENS, T. A. LOVE, and G. L. MORGAN, “Gamma Ray Production Due to Interactions with Aluminum for Incident Energies Between 0.85 and 20 MeV,” ORNL-TM-4232, Oak Ridge National Laboratory (1973).
 30. J. K. DICKENS, T. A. LOVE, and G. L. MORGAN, “Gamma Ray Production from Neutron Interactions with Silicon. . . ,” ORNL-TM-4389, Oak Ridge National Laboratory (1973).
 31. G. L. MORGAN and D. C. LARSEN, “The Ti($n, x\gamma$) Reaction Cross Section for Incident Neutron Energies Between 0.3 and 20.0 MeV,” ORNL/TM-6323, Oak Ridge National Laboratory (1978).
 32. G. T. CHAPMAN, G. L. MORGAN, and F. G. PEREY, “A Remeasurement of the Neutron-Induced Gamma-Ray Production Cross Sections for Iron in the Energy Range 850 keV $\leq E_n \leq$ 20.0 MeV,” ORNL/TM-5416, Oak Ridge National Laboratory (1976).
 33. G. L. MORGAN, “Cross Sections for the Cu(n, xn) and Cu($n, x\gamma$) Reactions Between 1 and 20 MeV,” ORNL-5499, Oak Ridge National Laboratory (1979).
 34. J. K. DICKENS, T. A. LOVE, and G. L. MORGAN, “Gamma-Ray Production Due to Neutron Interactions with Tungsten. . . ,” ORNL-4847, Oak Ridge National Laboratory (1973).
 35. G. L. MORGAN and E. NEWMAN, “The Au($n, x\gamma$) Reaction Cross Section for Incident Neutron Energies Between 0.2 and 20.0 MeV,” ORNL-TM-4973, Oak Ridge National Laboratory (1975).
 36. G. T. CHAPMAN and G. L. MORGAN, “The Pb($n, x\gamma$) Reaction for Incident Neutron Energies Between 0.6 and 20.0 MeV,” ORNL-TM-4822, Oak Ridge National Laboratory (1975).
 37. G. N. MASLOV, F. NASYROV, and N. F. PASHKIN, *At. Energ.*, **24**, 573 (1968).
 38. V. C. ROGERS, D. COSTELLO, D. R. DIXON, C. G. HOOT, and V. J. ORPHAN, “Gamma Ray Production Cross Sections for Silicon and Copper from Threshold to 20 MeV,” DNA 3818E, Defense Nuclear Agency (1975).
 39. P. RAMAKRISHNAN, G. E. MITCHELL, C. R. GOULD, S. A. WENDER, and G. F. AUCHAMPAUGH, *Nucl. Sci. Eng.*, **98**, 348 (1988).
 40. K. SUGIYAMA, “Status of Gamma Ray Production Cross Section Data,” *Proc. Int. Conf. Nuclear Cross Sections and Technology*, Knoxville, Tennessee, October 22-26, 1979, p. 397 (1980).